CHAPTER-6

ELECTRICAL RESISTIVITY METHOD

6.1 Introduction

Introducing current into the ground for prospecting purposes started about a century ago. From the historical point of view, the initial application of the electrical resistivity method in geophysical prospecting began with the work of Wenner (1915) and Schlumberger (1920), who proposed a four-point electrode configuration for field measurements, which revolutionized geophysical exploration in this field. A third general class of electrode arrays is the dipole-dipole class described by Al'pin (1950) for deep investigations. The electrode arrays used by Wenner and Schlumberger became very popular and are still in vogue. The development of different techniques of resistivity data interpretation led to its extensive application in exploration activities, especially for delineating groundwater resources. Vertical electrical sounding (VES) can also be used to determine the aquifer depth. aquifer geometry hydraulic conductivity, the water quality of the aquifer rock, and geological stratigraphy as reported by many researchers such as Chandra et al.(2008); Robinson (2012); Mohamaden et al.(2016); Mahmoud and Ghoubachi (2017).

6.1.1 Definition of Resistivity

Resistivity, symbolized as ρ, represents a physical characteristic of a material, similar to density. It serves as an intrinsic property of a substance, unaffected by the substance's dimensions or configuration. Let's look at a substance having a regular shape, like a cylinder, to understand the concept of resistivity as shown in Figure 6.1

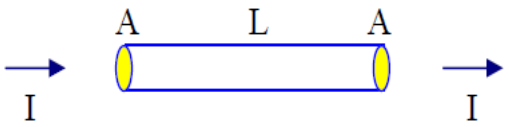

Figure 6.1 A regular shape cylinder

The resistance offered by this cylinder can be written as

$$R = \frac{\rho L}{A} \tag{6.1}$$

Where, R = Resistance offered by the cylinder

L = Length of the cylinder

A = Area of a cross-section of the cylinder

ρ = resistivity of the substance

Arrows show the direction of the current. By rearranging equation (6.1), we get:

$$\rho = \frac{R \times A}{L} \tag{6.2}$$

If we assume L and A unity, then

$$\rho = R$$

As a result, the resistivity of a substance is defined as the resistance exhibited by a substance with a unit length and a unit cross-sectional area. In the case where the meter is used as the unit of length and ohm as the unit of resistance, then units of resistivity are determined as

$$\frac{\text{Metre}^2(\text{L}^2) \times \text{ohm}(\text{R})}{\text{Metre}(\text{L})} = \text{ohm} \times \text{metre} \tag{6.3}$$

The inverse of resistivity is known as conductivity (σ), while the inverse of resistance is known as conductance.

6.2 Theoretical background of the resistivity method

6.2.1 General introduction

The basis of the resistivity method involves introducing an artificially generated electric current into the ground, and the resulting potential differences are measured at the surface. Any subsurface variation in conductivity changes the current flow within the earth, affecting the distribution of electrical potential measured at the surface (Telford et al. 1990). The electrical potential and current measured on the earth's surface can provide information on the resistivity variation of the subsurface in any particular area. Often, it is difficult to relate these measured quantities to subsurface resistivity stratification. Many techniques have been employed to derive this relation, relying on several assumptions. However, it must be noted that determining resistivity may solve an electric problem but may not necessarily be a geological one, as certain geological formations are not related to specific resistivities except in a broad and general sense (Parasnis, 1979).

The collection and interpretation of electrical resistivity measurements are based on the fundamental principle derived from Ohm's Law, which is a fundamental theory in physics governing the flow of electrical current in a conductor. Ohm's Law states that the current passing through a conductor is directly proportional to the voltage applied across it i.e.

$$V = I * R \tag{6.4}$$

The equation for Ohm's Law in vector form for current flow in a continuous medium is given by

$$J = \sigma * E \tag{6.5}$$

Where, J = Current density

σ = Conductivity of the medium

E= Electric field intensity

In geophysical surveys, the reciprocal of the conductivity ($\sigma = 1 / \rho$) is the resistivity ρ, which is a more commonly used parameter for surveys.

The field intensity, E can be described by the gradient of the potential field as

$$E = -\nabla . V \tag{6.6}$$

Combining equations (6.5) and (6.6)

$$J = -\sigma \nabla . V = -\frac{1}{\rho} \nabla . V \tag{6.7}$$

The simplest approach to this theory is to apply the following boundary conditions given by Koefoed (1979).

I. The subsurface consists of a finite number of layers that are separated by horizontal boundaries. The deepest layer of which extends to an infinite depth.
II. Electrical homogeneity and isotropy both exist within each layer.
III. A point source of current at the earth's surface produces the field.
IV. The source emits a direct current.

Considering the above boundary conditions and applying divergence conditions to Equation (6.7) such as

$$\nabla . J = \nabla . (\sigma \nabla . V) = 0$$

$$\nabla . J = \nabla . \sigma \nabla V + \sigma \nabla^2 V = 0 \quad (6.8)$$

If, σ is the constant throughout

$$\nabla^2 V = 0 \quad (6.9)$$

The resistivity method is established where the potential field resulting from a flow of current may be described by a solution of Laplace's equation which satisfies the above boundary conditions.

6.2.2 Potential distribution over a stratified earth caused by a point current source

The primary goal of electrical prospecting is to identify the depth and electrical resistivity of horizontal or nearly horizontal strata. The apparent resistivity measured is generally a function of a variable related to the depth of current penetration. It is equivalent to true resistivity only when the subsurface is homogeneous. However, such a condition is difficult to obtain, so a more convenient way of expressing a response to the actual distribution of vertical resistivity is to assume the subsurface is divided into thin strata, with each stratum considered wholly homogeneous and isotropic (Koefoed, 1979). The cylindrical coordinate system with the point source of current P at the origin and the Z-axis vertically downward normal to the surface is chosen in this situation (Figure 6.2). Current I is placed on the surface of the n-layered horizontal earth, having the resistivities ρ_1, ρ_2,.... ρ_n and thickness

h_1, h_2,…h_n with the respective depth of d_1, d_2 . . . d_n from the top to the bottom of each layer. The bottom layer is assumed to have a depth that extends to infinity, i.e., h_n and $d_n \rightarrow \infty$.

The potential arising from any number of horizontal layers is derived from the solution of the cylindrical coordinate representation of Laplace's equation. The electrode is taken as the origin of the polar coordinate system, with the vertical line as the Z-axis positive downward and the r-axis in a plane parallel to the surface of the earth as shown in Figure 6.2. In the cylindrical coordinate system, the potential V must satisfy Laplace's equation everywhere except at the electrode (due to symmetry about Φ) given by

$$\nabla^2 V = \frac{\partial^2 V}{\partial r^2} + \frac{1}{r}\frac{\partial V}{\partial r} + \frac{\partial^2 V}{\partial z^2} = 0 \qquad (6.10)$$

Equation (6.10) Laplace's equation in cylindrical coordinates has only the r and z terms and this differential equation can be solved by Fourier's method, by assuming a solution as

$$V(r, z) = U(r), W(z) \qquad (6.11)$$

Where U(r) is a function of r and $W(z)$ is a function of z only, each solution being independent of the other.

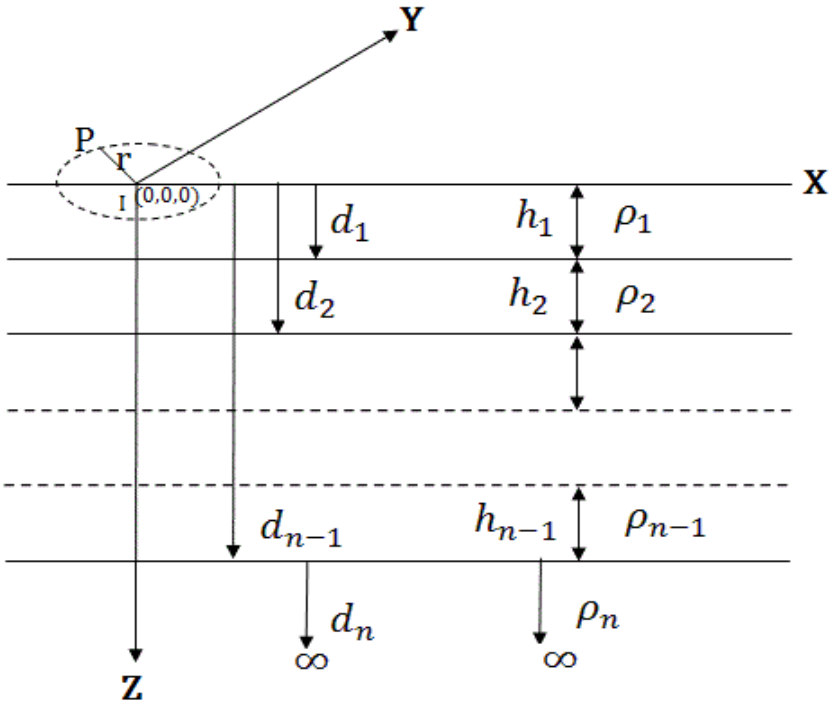

Figure 6.2 A potential source kept at the surface of the layered earth.

In the situation of a point source of current at the surface of horizontally layered earth, separate expressions for the general solution in the different layers may therefore be written (Koefoed, 1979) as

$$V_i = \frac{\rho_1 I}{2\pi}\int_0^{\infty}\left[e^{-\lambda z} + A_i(\lambda)e^{-\lambda z} + B_i(\lambda)e^{\lambda z}\right]J_0(\lambda r)d\lambda \qquad (6.12)$$

For the adoption of the solution, the following boundary and continuity conditions must be satisfied, such as

I. Across interfaces, the potential must be continuous and finite.

II. Across the interfaces, the normal component of current density is also continuous.

III. Since air has infinite resistance, the vertical component of potential at the surfaces must be zero.

IV. At great distances from the current electrode, the potential vanishes.

After taking above the boundary and continuity conditions, Stefanesco and Schlumberger (1930) derived the electrical potential at the surface (z = 0) for a series of horizontal layers, the uppermost of which having a resistivity at a distance r from the current source of strength, I is in the form of Henkel's integral as

$$V(r) = \frac{I\rho_1}{2\pi r}\left[1 + 2r\int_0^\infty \theta(\lambda, k, h).J_o(\lambda, r)d\lambda\right] \qquad (6.13)$$

Where,

$\theta(\lambda, k, h)$ = Kernel function, determined by thickness and resistivities of the enclosed layers of the subsurface under consideration,

$J_o(\lambda, r)$ = Bessel function of zero order and first kind,

λ = Integration variable having the dimension of inverse length.

The expression under the integral is known as the Stefanesco function and is vital in electrical resistivity sounding. Stefanesco solved the problem for two, three, and four layers. Flathe (1955) developed a mathematical formulation for the kernel function in terms of depth and resistivities of the subsurface for six layers. Pekeris (1940) and Flathe (1955) presented recurrence relations by which the kernel for the different number of layers could be evaluated from its preceding one. The two recurrence relations are different from each other. Flathe recurrence relation adds a new layer at the bottom of the original layer sequence.

In contrast, Pekeris's recurrence relation adds a new layer at the top of the original layer sequence and, at the same time, moves the electrode configuration to the top of the newly added layer. It may also be applied in the reverse direction, known as a reduction to a layer boundary, by removing the top layer and, at the same

time, lowering the electrode configuration to the top of the second layer. When reducing to a lower boundary, the starting function must correspond with the observation on the top of the original layer sequence, which must be derived from the field observation. The Flathe and Pekeris recurrence relations have specific fields of application. However, in some applications, either of them may be used; in such applications, the Pekeris recurrence deserves preference because of its more straightforward and reversed structure (Koefoed 1979).

6.2.3 Resistivity Kernel Functions and Recurrence Relations

Slichter (1933) introduced a function (λ) in the potential expression, which is related to Stefanesco's kernel function $\theta(\lambda)$ and is given as,

$$\mathrm{K}\,(\lambda) = 1 + 2\theta\,(\lambda) \tag{6.14}$$

Koefoed (1970) introduced a new function called the raised kernel function which is given by,

$$\mathrm{T}\,(\lambda) = \rho_1 K\,(\lambda) \tag{6.15}$$

The resistivity transforms function $T\ (\lambda)$ is also related to the resistivities and thicknesses of the sub-surface layers like other kernel functions. The original form of Pekeris's (1940) recurrence relation has been replaced by Koefoed (1979) in terms of resistivity transform function (λ), and it is given as,

$$T_i(\lambda) = \frac{\rho_i[T_{i+1}(\lambda) + \rho_i \tanh\,(\lambda h_i)]}{\rho_i - [T_i(\lambda)\tanh\,(\lambda h_i)]} \tag{6.16}$$

The dimension of the resistivity transform is similar to that of resistivity. The resistivity transform (T) is a function of λ, and λ has a dimension reciprocal of length. The resistivity transforms (T) and apparent resistivity (ρ_a) as a function of electrode spacing have some analogies due to the asymptotic behavior. It has been observed that the resistivity transform and apparent resistivity show the same asymptotic behavior for both large and small abscissa values.

Further, the details on the recurrence relation can be seen in the study of Roman (1963), Szaraniec (1980), and Keofoed (1979). The resistivity transform curve for the known geological model can be computed using the equation (6.16). The expression for Schlumberger's apparent resistivity and resistivity transform can be given as,

$$\rho_{as} = s^2 \int_0^\infty T(\lambda) J_1(\lambda s) \lambda d\lambda \tag{6.17}$$

The explicit expression for resistivity transform (T), which is of fundamental importance, is used to determine the function at an intermediate step in interpreting resistivity field data. T(λ) can be obtained by applying Hankel's inversion theorem of the Fourier-Bessel integral to the equation (6.17) as follows:

$$T(\lambda) = s^2 \int_0^\infty \rho_{as}(s) J_1(\lambda s) \frac{ds}{s} \tag{6.18}$$

By observing equations (6.17) and (6.18), we found that there is a relation between resistivity transform functions and apparent resistivity, as both equations are linear. Based on this relation Ghosh (1970) introduced the application of a digital linear filter to resistivity-sounding data.

6.2.4 Computation of Theoretical Curves

There are four methods for the computation of theoretical curves:

- The computation of theoretical apparent resistivity curves could be done using the numerical integration method based on evaluating an integral expression. The infinite integral is replaced by finite integrals and numerically integrated. For the computation of model curves published by Mooney and Wetzel (1956), the sections of the resistivity transform function are approximated by second-degree polynomials.
- Van Dam (1967) and Mooney et al. (1966) have used the infinite series expansion method for the computation of theoretical curves.
- Flathe (1955) described the decomposition method into partial fractions based on the assumption that the thicknesses of all layers are integral multiples as a common reference thickness.
- Ghosh (1970 and 1971) developed a digital linear filtering method to compute theoretical curves with known sampled values of resistivity transform (calculated from the layer parameters) and digital inverse linear filters. Resistivity transform values at required sampling intervals are computed using the Pekeris recurrence relation (Equation 6.16) for any number of layers. Then the sampled apparent resistivity can be calculated using the following equation:

$$\rho_{as}(X_i) = \sum_{j=-NN}^{NP} a_j T(Y_i - j\Delta Y) \qquad (6.19)$$

Where NN and NP are the numbers of filter points to the left and right side of filter coefficient a_0, respectively, and $T(Yi - j\Delta Y)$ is the resistivity transform value at abscissa $(Yi - j\Delta Y)$; Yi is the abscissa corresponding to filter Coefficient a_0 .

6.2.5 The Principles of Resistivity method and field procedures

To compute the potential distribution in layered earth, first calculate the normal potential at the earth's surface due to a point source of current placed over a homogeneous ground, as shown in Figure 6.3.

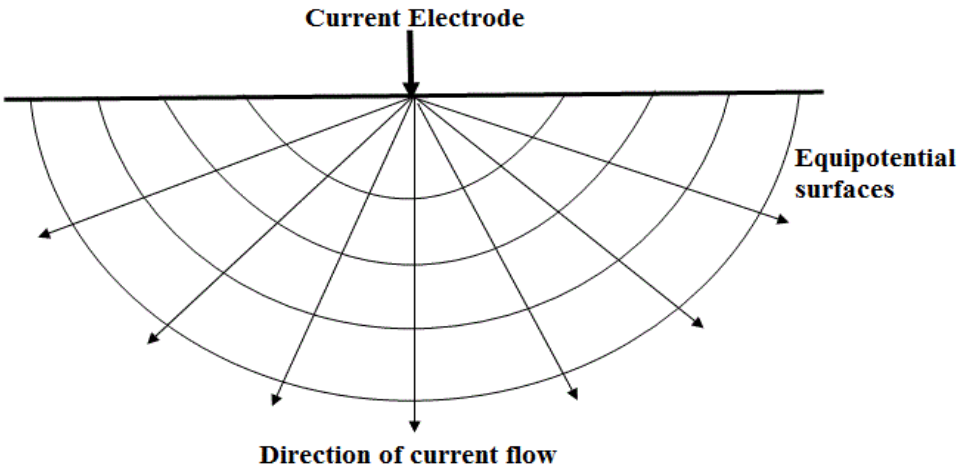

Figure 6.3 Current flow from a single source electrode (Telford et al., 1976).

The general form of electrode layout used in resistivity measurement consists of two current electrodes C_1 & C_2, and two potential electrodes P_1 & P_2, as shown in Figure. 6.4.

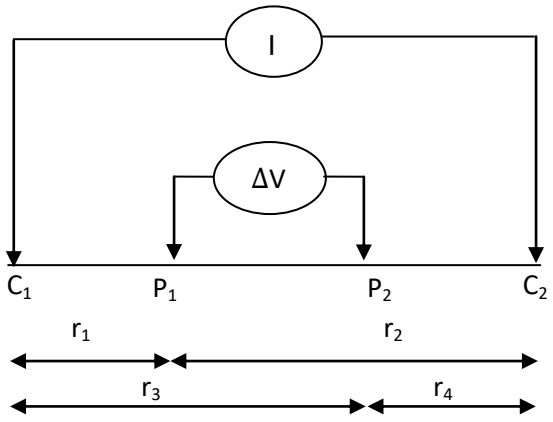

Figure 6.4 Two current and two potential electrodes on the surface of homogeneous isotropic ground of resistivity (Telford et al. 1976).

The potential V_{P_1} at the internal electrode P_1 is the summation of the potential contributions from current electrodes C_1 and C_2, and the potential V_{p_2} is the sum of

the potential contributions from current electrodes C_1 and C_2 at another internal electrode P_2.

$$V_{P_1} = \frac{\rho I}{2\pi}\left(\frac{1}{r_1} - \frac{1}{r_2}\right) \tag{6.20}$$

$$V_{p_2} = \frac{\rho I}{2\pi}\left(\frac{1}{r_3} - \frac{1}{r_4}\right) \tag{6.21}$$

The measured potential difference by a voltmeter connected between P_1 and P_2 is

$$\Delta V = V_{P_1} - V_{P_2}$$

and rearranging the terms, then it becomes

$$V = \frac{\rho I}{2\pi}\left(\frac{1}{r_1} - \frac{1}{r_2} - \frac{1}{r_3} + \frac{1}{r_4}\right) \tag{6.22}$$

Since Earth is not homogeneous and isotropic, the measurement of ρ can be represented by ρ_a.

Hence,

$$\rho_a = G\frac{\Delta V}{I} \tag{6.23}$$

Where, $G = 2\pi \frac{1}{\left(\frac{1}{r_1} - \frac{1}{r_2} - \frac{1}{r_3} + \frac{1}{r_4}\right)}$ which represents geometrical for the layout mentioned above.

This resistivity across the homogeneous isotropic medium will be constant for any current electrode arrangement. The measured property is known as "apparent resistivity" for an inhomogeneous material (layered earth). The apparent resistivity of a geological formation, as measured for a specific electrode configuration and current

strength (I), can be considered as the true resistivity of an imaginary homogeneous and isotropic medium, for which the measured potential difference (ΔV) is equivalent to that obtained for the actual inhomogeneous medium being considered (Koefoed, 1979). The value of the apparent resistivity is influenced by the geometry and resistivity of the elements present in the geological medium under consideration.

(i) Wenner Configuration

Wenner (1915) simplified the distance AB to be 3*a* means, *a* is the spacing between two consecutive electrodes as shown in Figure 6.5(a). Putting the value of r_1, r_2, r_3, and r_4 in terms of *a* in equation (6.16) then the potential difference in the array can be written as

$$\Delta V = \frac{\rho I}{2\pi a} \tag{6.24}$$

Here again, ρ is not the true resistivity for measurement purposes over inhomogeneous ground and can be represented as ρ_{aW}.

This becomes

$$\rho_{aW} = 2\pi a \frac{\Delta V}{I} \tag{6.25}$$

Where 2πa is the geometrical factor for Wenner configuration.

(ii) Schlumberger configuration

Schlumberger (1920) made further simplification for linear four electrodes A, M, N, and B. The potential electrodes M and N potential electrodes are placed symmetrically about the center O of the spread AMNB. The spacing between M and

N is taken to be small at least 5 times less than the distance of current electrodes AB so that the potential gradient would be measured as shown in Figure 6.5(b). The potential difference for the Schlumberger array can be written as

$$\Delta V = \frac{\rho I}{2\pi}\left(\frac{2}{s-b} - \frac{2}{s+b}\right) \tag{6.26}$$

Which gives apparent resistivity ρ_{aS} as

$$\rho_{aS} = \left(\pi\frac{s^2 - b^2}{2b}\right)\frac{\Delta V}{I} \tag{6.27}$$

The quantity in the bracket is the geometrical factor for the Schlumberger configuration.

(a)

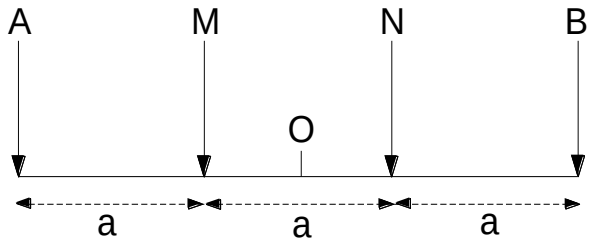

(b)

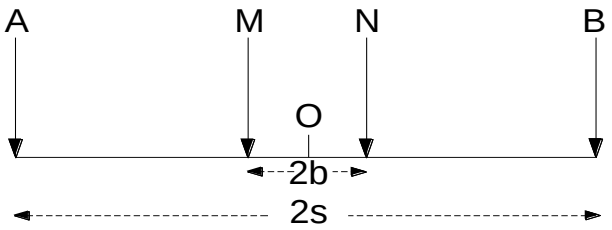

Figure 6.5 (a) Symmetrical electrode arrangement of Wenner array, **(b)** Schlumberger array (Telford et al. 1976).

The electrical resistivity surveys are carried out in two ways, known as (i) Resistivity profiling and (ii) Resistivity sounding. Resistivity profiling is used to

detect lateral changes in resistivity for a particular depth, depending on the electrode separation used and a constant setup (separation) of electrodes is placed at various points of observation along a profile. The resistivity sounding is carried out to detect the changes in resistivity with depth in earth sections and interpret them in terms of geological and hydrogeological conditions. In geosounding, the electrode separations are increasing in steps while keeping the center point of array is fixed (Al'pin, 1950; Keller and Frischknecht, 1966; Kunetz, 1966; Bhattacharya and Patra, 1968; Koefoed, 1979, Telford, 1988, 1990; Sharma, 1997; Parasnis, 1979). Some other configurations were developed by Das and Verma (1980); Das and Singh (1982); Yadav and Singh (1983); and Yadav (1988) for the resistivity survey.

6.2.6 Dar-Zarrouk Parameters for Aquifer characterization

Dar- Zarrouk Parameters are a set of variables that may be used to define the geoelectrical characteristics of each unit in a layered section (Maillet,1947). According to Zohdy et al. (1974), this parameter consists of the following values: total longitudinal resistivity, total transverse resistivity, total longitudinal unit conductance (S), total transverse unit resistance (T), and Coefficient of anisotropy.

Considered a layered model, as shown in Figure 6.6, the transverse resistance (T) is determined by multiplying the resistivity and thickness of each layer, while the longitudinal conductance is obtained by dividing the thickness of each layer by its resistivity. In the case of a series of n horizontal layers that are homogeneous and isotropic, with resistivity ρ_i and thickness h_i, the Dar-Zarrouk parameters are defined as:

$$S = \sum_{i=1}^{n} \frac{hi}{\rho i} (mohos) \tag{6.28}$$

$$T = \sum_{i=1}^{n} \rho i \times hi \ (ohm - m^2) \tag{6.29}$$

Combining equations (6.28) and (6.29) leads to the definition of total transverse resistivity, ρ_t, as the total transverse resistance, T, divided by the total thickness of the layers, H:

$$\rho_t = \frac{T}{H} \ (ohm - m) \tag{6.30}$$

And total longitudinal resistivity, ρ_l, is defined as the total thickness, H, of the layers divided by the longitudinal conductance, S:

$$\rho_l = \frac{H}{S} (ohm - m) \tag{6.31}$$

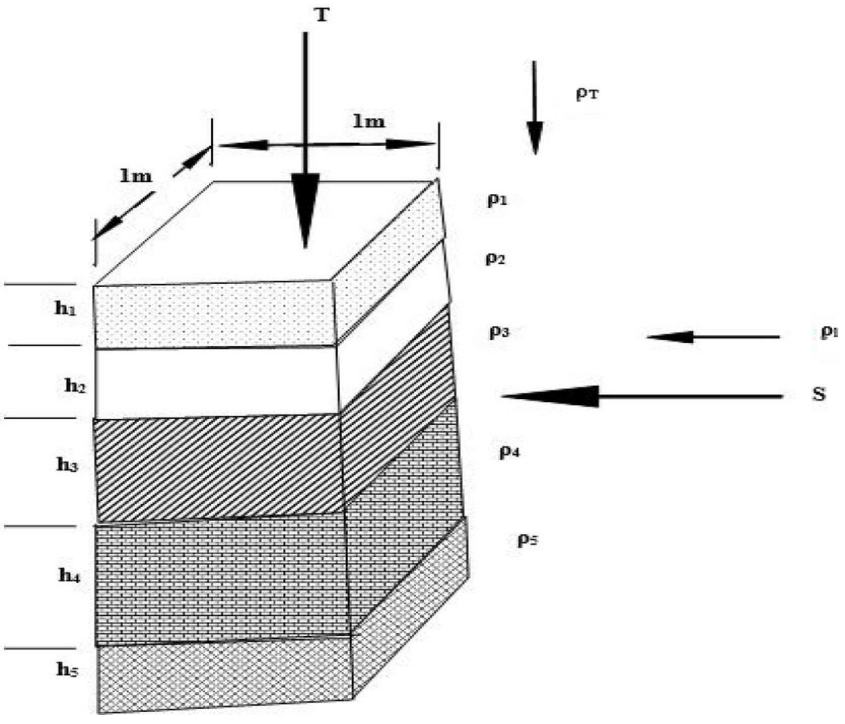

Figure 6.6 Layered model showing longitudinal conductance (S) and transverse resistance (T).

Based on the Dar-Zarrouk parameters, Maillet (1947) finds the expression for the Coefficient of anisotropy, λ as:

$$\lambda = \sqrt{\frac{\rho_t}{\rho_l}} \tag{6.32}$$

The Coefficient of anisotropy generally lies between 1 to 2 and may often sometimes exceed 2.0 (Zohdy et al. 1974). The Coefficient of anisotropy increases along with the hardness and compaction of the rock, leading to low porosity and permeability in these regions (Keller and Frischknecht 1966). It may be used to map groundwater zones with high porosity and a permeability layer and to determine the competence of the underlying material (Rao et al. 2003).

In hard rock formation, the variation in the value of T and S indicates the predominance of resistive or conductive zones above the basement rock. Up to the depth of the investigation, it estimates the sandiness or clayiness. As a result, it reveals lithological or groundwater variation in the area. Areas with high T and low S values can be inferred zones of high groundwater potential. Braga de Oliveira et al. (2006) states that sites with a low value of S are likely to have lower contamination risks.

These parameters are also used in inferring the hydrological properties of the aquifers. The similarity between T and transmissivity represents the possibility of the relation between these two parameters. Some authors, Croft (1971), Heigold et al. (1979), Niwas and Singhal (1981 and 1985), Frohlich and Kelly (1988), and Yadav (1995), etc., have represented the possibility of determining the transmissivity from the surface resistivity measurements.

6.3 Method for interpreting Geoelectrical data

The electrical resistivity method possesses a complex theoretical basis, so it is one of the most difficult geophysical techniques to interpret quantitatively (Barker, 2007). Flathe (1955) observed that the geological interfaces may not always be associated with the changes in lithological characters, and getting a proper correlation may become difficult. Because of variations in groundwater quality, a lithological unit may include several geological interfaces without any variation in character. The interpretation of the electrical resistivity method is divided into a type like other geophysical surveys (i) Qualitative interpretation method (ii) Quantitative interpretation method.

After completing the VES measurements, the quantitative interpretation method is commonly employed. This method provides general information about an area's geological structure and hydrogeological conditions and visualizes the changes in the geoelectrical section. The qualitative interpretation of sounding curves involves visually examining the curves to determine their "type" and delineating regions with similar curve characteristics. These types include ascending ($\rho_1 < \rho_2$), descending ($\rho_1 > \rho_2$), type or H ($\rho_1 > \rho_2 < \rho_3$), A ($\rho_1 < \rho_2 < \rho_3$), K ($\rho_1 < \rho_2 > \rho_3$) and Q($\rho_1 > \rho_2 > \rho_3$), which correspond to different combinations of resistivity variations in three-layer or multi-layered subsurface structures. The presence of highly resistive bedrock, representing the thickest and bottom-most geoelectrical layer, is indicated by a 45-degree slope in the last segment of the curve. Conversely, a highly conductive bottom layer is characterized by a steeply descending last segment (Telford et al., 1976).

The interpretation techniques are classified into two viz; indirect and direct methods depending on the process through which the layer parameters are deduced from the sounding curve.

6.3.1 Direct method of interpretation

The geo-electrical layer parameters can be obtained directly from the geo-electrical sounding data using the direct interpretation method (Langer, 1933). To obtain the layer distribution directly from field data, different attempts have been made by Slichter (1933), Van Nostrand and Cook (1966), and Vozoff (1958). There are two categories of direct interpretation of VES data: In the first category, the evaluation of resistivity transform (or kernel function) curve using a direct filter is described developed by Strakhov and Karelina (1969), Ghosh (1971) and Koefoed (1979). Pekeris (1940) and Koefoed (1979) formulas are used to interpret the resistivity transform curve, whereas, in the second category, the method of direct interpretation includes inversion of the sounding curve prior to transforming it in the resistivity transform curve (Rocroi, 1975; Patella, 1975; Zohdy, 1975; Drecun and Ketelaar, 1976).

6.3.2 Indirect method of interpretation

In this technique, the comparison of field sounding curve and theoretically obtained master curve for known layer parameters are made. Orellana and Mooney(1966), and Rijkstwaterstaat (1969) published two three and four layers standard master curves, and these master curves are widely used for the interpretation of resistivity-sounding curves. The indirect method of interpretation is uncomplicated,

relatively accurate, and frequently used for the quick understanding of geo-electrical sounding data. The practical procedures used in this technique of interpretation are:

(i) Complete curve matching

(ii) Partial curve matching

The complete curve matching provides the best results for determining geo-electrical layer parameters for a sufficiently thick layer. In this method, the field curve is plotted on transparent bi-logarithmic graph paper, and an appropriate master curve is selected from the sets of the master curve. The field curve is matched with the master curve until a good match is obtained, keeping the axis parallel to it. The origin of the master curve is marked on the bi-logarithmic graph paper, and the corresponding curve is marked. From this, the resistivities of the first, second, and third layers and thicknesses of the first and second layers can be obtained. The best matching represents that the layer parameters from the field data would be the same as indicated in the theoretical curve.

In partial curve matching, the small segment of the field curve is matched with the theoretical curve of two horizontal layers. In this method, auxiliary point charts are used to interpret resistivity-sounding data; therefore, it is also known as the auxiliary point method. Detailed discussions of this technique of interpretation are given in Hummel (1933), Ebert (1943), Zohdy (1965), Keller and Frischknecht (1966), Orellana and Mooney (1966), Kunetz (1966), Bhattacharya and Patra (1968) and Koefoed (1979).

6.3.3 Computer-assisted interpretation technique

The automatic iterative interpretation techniques are quick and relatively more accurate than the time-consuming manual interpretation of data. In this technique, the field data are compared with the data obtained from the layer model. The parameters of the layer model are adjusted if the two sets of data are found unsatisfactory, and the process is repeated until a good agreement is found between the two sets of data. The extensively used iterative interpretation methods are (Pekeris, 1940; Householder, 1953; Vozoff, 1958; Meinardus, 1970; Marsden, 1973; Zohdy, 1974; Patella, 1975; Johansen,1977) for the interpretation of geo-electrical sounding data. Yadav (1995) developed the "Automatic Iterative Method of Resistivity Sounding Interpretation" (AIMRESI) computer program for the interpretation of resistivity sounding.

6.3.3.1 Implementation of Genetic Algorithm

Implementing Simple Genetic Algorithms (SGAs) as a global optimization technique, a MATLAB-based program is developed to interpret 1-D resistivity sounding data for Schlumberger electrode configuration. This program can be used for any optimization problem by changing the response calculations. In this work, the forward response for Schlumberger electrode configuration is calculated using Ghosh's inverse filter method. Details of the developed MATLAB-based program are discussed in Chapter 5.

6.4 Delectability and ambiguity problems in the interpretation of VES data

Some inherent restrictions are associated with the resistivity method, and this causes ambiguity in the interpretation of sounding data. The instrument and techniques used in this method also result in an error of 3 to 5% (Keller and Frischknecht, 1966). The problem of equivalence and suppression is described below.

6.4.1 Problems of Equivalence

In the case of a multilayered geo-electrical sequence having a comparatively thin intermediate layer, the layer parameters (resistivity and thickness) of this thin layer can be altered to some extent, keeping either the product of resistivity and thickness or ratio of thickness to resistivity constant. This would not result in any detectable or appreciable differences in the sounding curve within the accuracy of the observation, and this phenomenon is known as equivalence. Pylaev (1948) discussed the problem of equivalence in detail and gave nomograms for all four types of three-layer sections. The K-type or Q-type curves are equivalent to transverse resistance, and the A-type or H-type curves are equivalent to longitudinal conductance. To deal with these problems, prior knowledge of the study areas' expected value of resistivities and thicknesses of subsurface formations must be known.

6.4. 2 Problems of Suppression

The problem of suppression is associated with continuously increasing or decreasing apparent resistivity (A-type or Q-type) curves as a function of electrode spacing. The thin intermediate geo-electrical layer is not reflected in the resistivity-sounding curve, even with different resistivity values. In such cases, a three-layer section may appear as two layers. The small thickness of the intermediate bed does not show any significant changes in the resistivity curve; however, its effect will start to appear on the resistivity-sounding curve when the thickness of the intermediate layer increases. Therefore, the interpreter often fails to identify the layer of intermediate resistivity, and this problem is repetitively encountered in groundwater studies.

6.5 Conduction of electricity through rocks:

In rock formations, three types of electric conduction may occur. They are electronic, ionic, and dielectric conductions. The magnitude of rock resistivities varies from a fraction of ohm-m to several thousands of ohm-m. Rocks containing a large concentration of metallic minerals and saline water may have resistivities ranging from 1 ohm-m to a few ohm-m. The marls and clays show one to a few tens of ohm-m. Sandstones and sand show from ten to a few hundred ohm-m. Figure 6.7 shows the general range of resistivities for some common rocks, soils, and ores. The resistivity of a particular formation varies with the degree of weathering and the number of fractures.

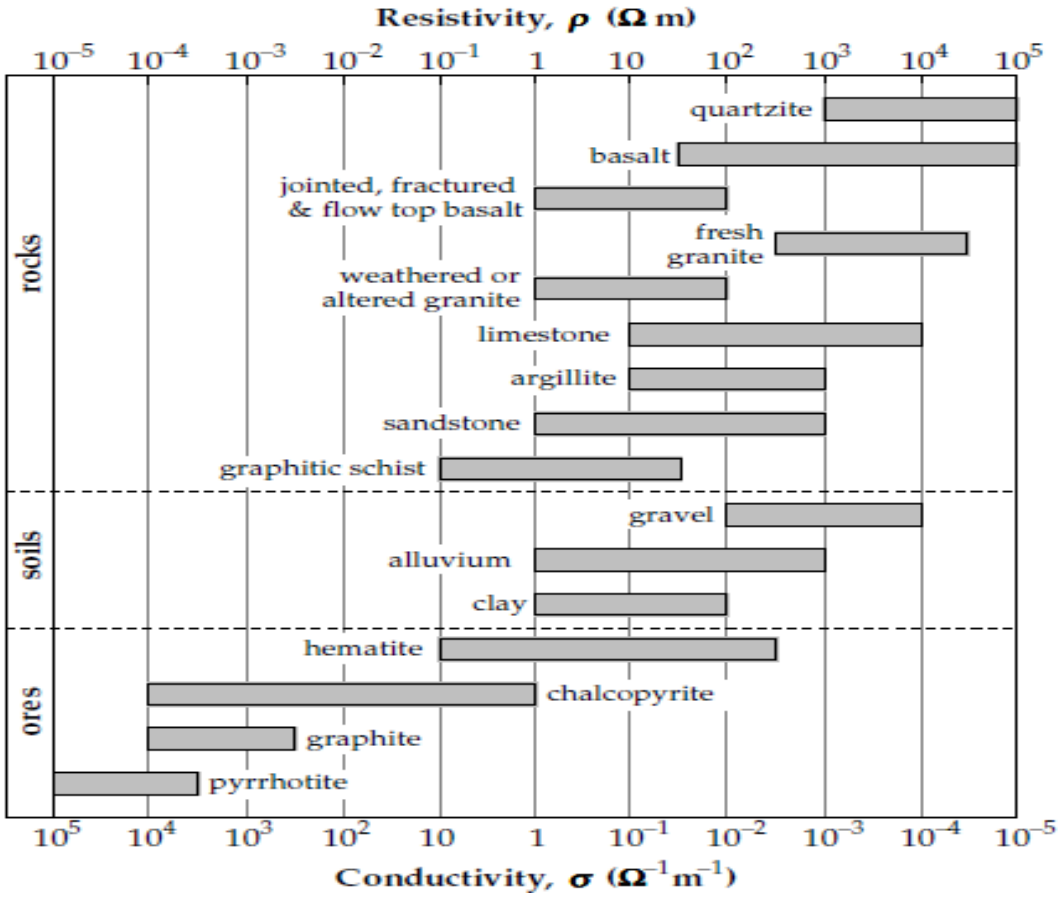

Figure 6.7 Electrical resistivity ranges for some common rocks, soils, and ores (Source: Ward, 1990; augmented by data from Telford et al.1990).

6.6 Resistivity Survey in the study area

The resistivity survey is conducted in the Singrauli coalfields region, Madhya Pradesh, India. For a successful resistivity survey, it is quite necessary to choose a suitable place of even topography because the electrical resistivity method is very sensitive to topographic effects. Care should be taken to avoid buried conductors such as pipelines, telephone cables, and oil and water tanks along the profile line.

6.6.1 Instrument and accessories

6.6.1.1 Instrument used

A resistivity survey is conducted by a device called a resistivity meter (depicted in Figure 6.8), which consists of a current generator and a voltmeter. To carry out the survey, a resistivity meter capable of producing direct current (DC) or very low frequency alternating current (AC) with an appropriate voltage is employed. Ideally, a DC source is needed, but it leads to electrode polarization and interference from natural potentials in the signal. Consequently, the polarity of the DC source must be reversed to eliminate these unwanted effects.

Figure 6.8 Resistivity meter (IGIS SSR-MP-ATS)

On the other hand, the alternating current (AC) source effectively eliminates the undesirable aspect of DC, and the ground impedance is measured instead of resistance. Presently, a low-frequency square pulse current is commonly used instead of DC instruments due to its numerous advantages. It is preferable for the current to have measurement accuracy in the micro-volt range. These instruments offer several features such as stacking capability, a digital display that shows direct resistivity/resistance or current input and measured voltage, built-in noise rejection, and line-continuity checking. Additionally, they provide the option to select constant voltage or constant current input. Some instruments even display the standard deviation for each measurement, which provides statistical confidence in the dataset.

In the study area, the SSR-MP-ATS resistivity meter manufactured by IGIS Hyderabad was utilized for data acquisition. The SSR-MP-ATS is an advanced microprocessor-based data acquisition instrument based on signal stacking known as Signal Enhancement Resistivity Meter. This instrument incorporates several new features and advanced digital circuitry techniques, making it a trustworthy tool for various geophysical applications, including mineral and groundwater exploration.

One distinguished feature of the SSR-MP-ATS is its ability to send the entire current into the ground without wasting power on the constant current generation. This efficient use of power increases the signal strength, enabling the instrument to investigate deeper layers. Despite the relatively low power inputs, the advanced design of the SSR-MP-ATS Resistivity Meter achieves excellent depth penetration.

The SSR-MP-ATS utilizes signal stacking, which involves combining up to 16 successive readings, resulting in significant signal enhancement. In the presence of

random earth noises that lack coherence, the signal-to-noise ratio of the SSR-MP-ATS measurement is enhanced by the square root of the number of stacks (denoted by N). Therefore, the SSR-MP-ATS Resistivity Meter can successfully be used for depths of up to 600m in favorable geological conditions.

6.6.1.2 Accessories for the resistivity survey

The resistivity survey required the following accessories.

- Four stainless steel rod stakes of 0.5 to 0.75 m in length of small diameter, one end should be sharp and pointed.
- Four hammers of 2 to 3 kg and four measuring tapes of 100 meters in length should be standard, rugged, and non-expandable plastic/nylon.
- Four rugged winches/reels have steel/aluminum frames and an insulated base. Each may have a 500 m cable of thick PVC insulated, single-conductor, multi-strand thin wires of low electrical resistance. The cable length depends on the maximum spread of sounding to be conducted.
- The eight crocodile clips of various sizes, banana pin connectors, and insulation tapes. A power source capable of producing direct current (DC) and can be recharged, or a power source with a converter, or a power generator with a converter, is required. The power source should be capable of producing a constant rated supply and allow for multiple range selection.
- A Brunton compass for measuring the dip and strike of the bed, ranging rods for fixing profile layout direction, and a GPS device for locating the VES station coordinates.
- Three hand-held walkie-talkie sets, of 4 km range.

6.6.2 Data acquisition in the field survey

In the present study, fifty-five VES data were acquired around coal mine projects colonies, in mines, and nearby villages in the vicinity of the mining area. Some photographs of data acquisition are shown in Figure 6.9.


REDMI NOTE 6 PRO
MI DUAL CAMERA
2020/10/30 10:54


REDMI NOTE 6 PRO
MI DUAL CAMERA
2020/11/3 15:57

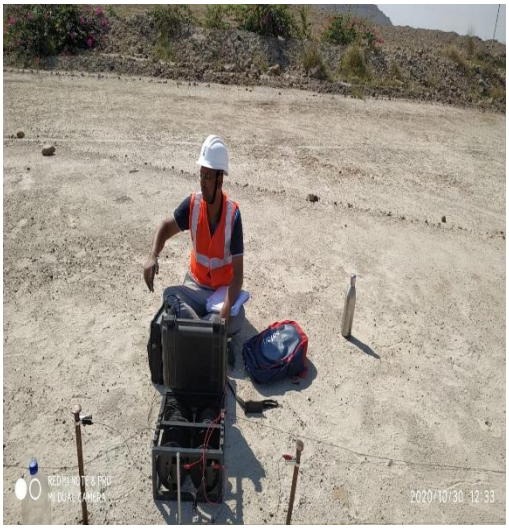

Figure 6.9 VES data acquisition in the Singrauli Coalfield region.

6.6.3 Vertical electrical sounding (VES)

Fifty-five VES data were collected using Schlumberger electrode configuration with a maximum current electrode separation (AB) of 400 m and distance used for the potential electrode spacing (MN) ranging from 1.0 m, 4.0 m, 10.0 m, and 20 m with spreading along north-south and east-west direction during the resistivity survey. The location of VES points and borehole is shown in Figure 6.10.

To conduct the VES (Vertical Electrical Sounding) survey, the Schlumberger configuration is used. This configuration involves four electrodes placed in a straight line. The spacing between the potentials and current electrodes is maintained at one-third to one-fifth of the total spacing. During the survey, the distance between the current electrodes is gradually increased, while the potential electrodes remain in their original positions. This process continues until the voltage becomes too small to measure accurately. This methodology was outlined in studies conducted by Keller and Frischknecht (1966) and Koefoed (1979). If AB ≥ 3MN, errors in apparent resistivity measurement would generally be within 2% to 3% (Van Nostrand and Cook, 1966).

In the present study, the field curves have been interpreted in two steps: In the first step, the sounding curves are analyzed indirectly by curve matching techniques using three-layer master curves of Rijkstwaterstaat (1969); and corresponding auxiliary point charts. In the second step, the data were interpreted with the help of a developed MATLAB-based program using a Genetic Algorithm. This work aims to evaluate the geohydrological layers and groundwater potential zones' using geoelectrical-sounding data.

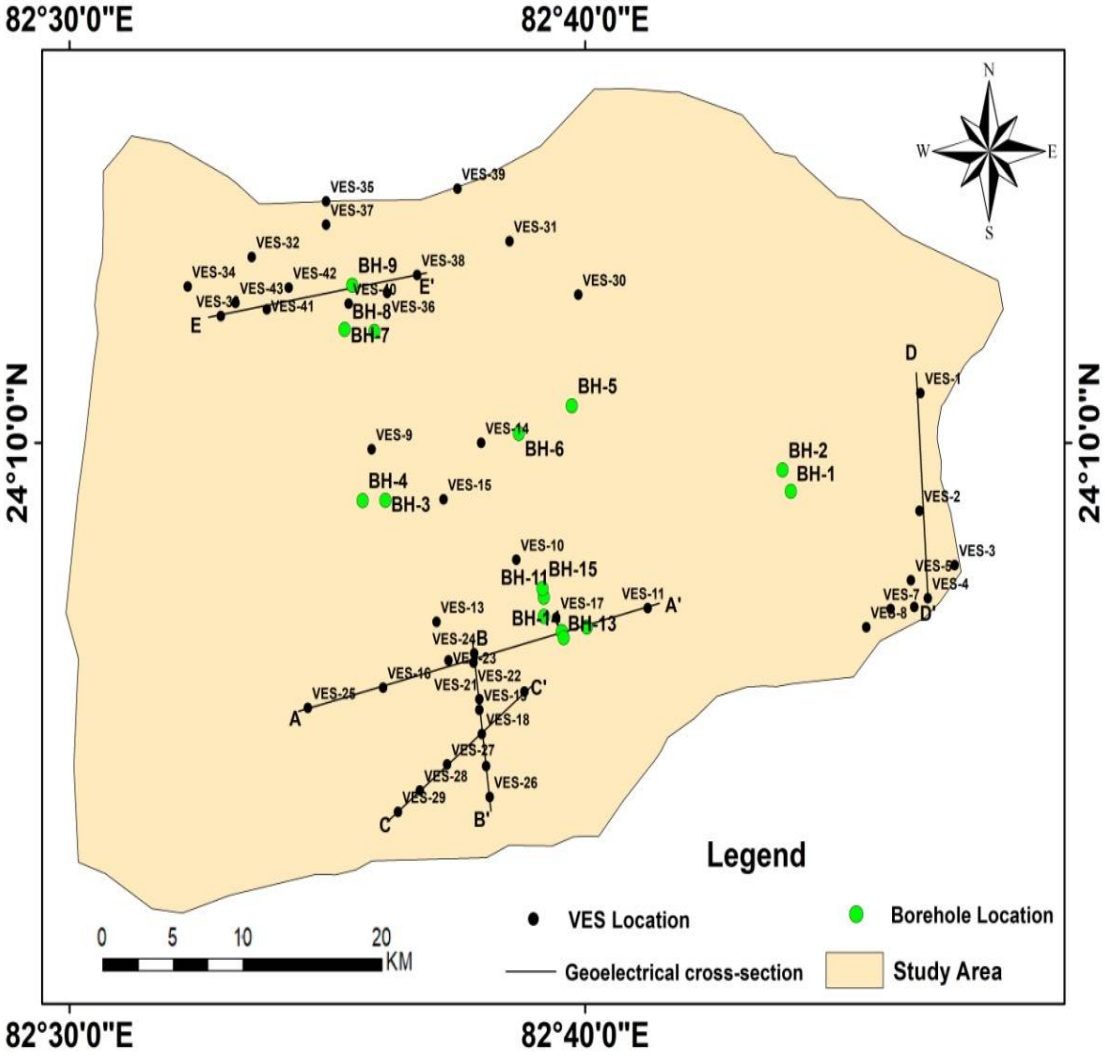

Figure 6.10 Investigation Map of resistivity survey of the study area.

6.6.3.1 VES for Aquifer Characterization around Gorbi mine.

The Gorbi mine is an abandoned mine situated north of the Singrauli Coalfield region. Out of a total of fifty-five VES, twenty-six were conducted in twenty-five villages around Gorbi mine, as shown in Figure 6.11 (a) and (b). This work aims to evaluate secondary parameters known as Dar-Zarrouk parameters for aquifer characterization and to find the protective capacity of overburdened rock materials.

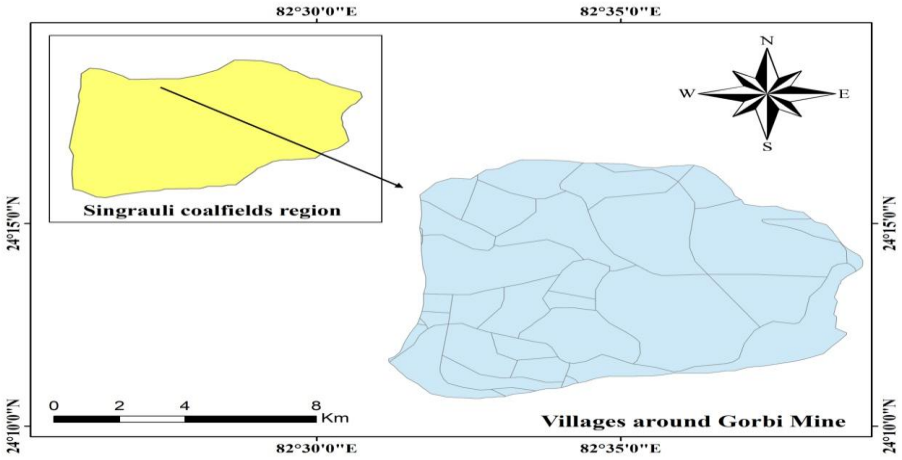

Figure 6.11 (a) Location Map of villages around Gorbi mines.

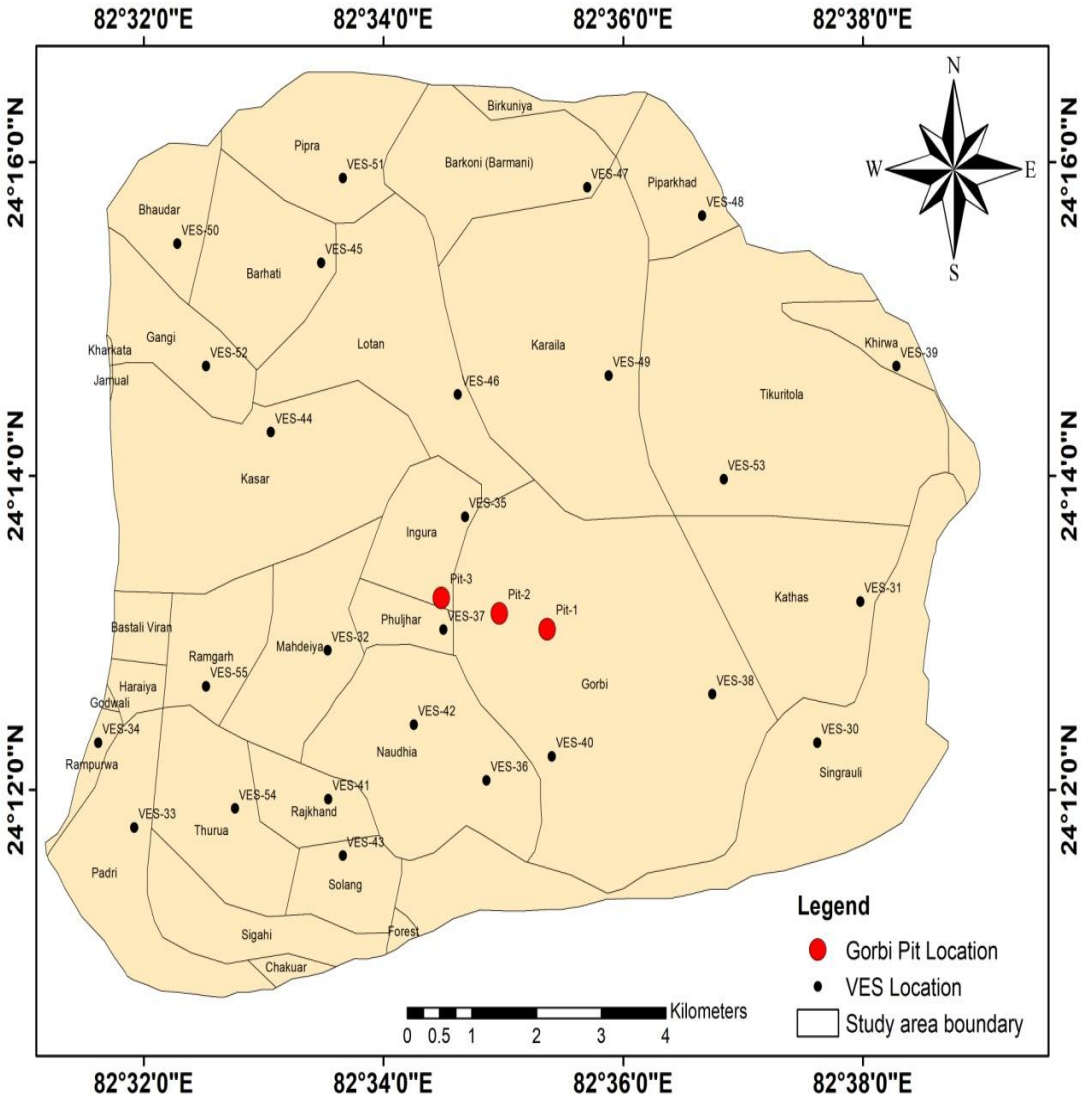

Figure 6.11(b) Map of VES location in villages around Gorbi mines.

6.7 Result and discussion

6.7.1 Vertical electrical sounding

A total of fifty-five VES were conducted, as per availability of space and accessibility of the area, and data were interpreted with the help of a developed MATLAB-based program using a Genetic Algorithm as described in chapter 5 and listed in **Appendix B**. To know the variation in the range of resistivity of the lithological units present in the study area, the interpreted results of VES data have been correlated with the available borehole data presented in the following subsection.

6.7.1.1 Correlation of geoelectrical layers parameters with existing boreholes lithology.

The layer parameters of VES-9, VES-10, and VES-40 correlated with the lithology of boreholes BH-4, BH-8, and BH-11, respectively.VES-9 and BH-4 are situated in the central portion of the study area, and VES-10 and BH-11situated south of the study area near Jayant Mine, whereas VES-40 and BH-8 are located north of the study area near block-B, Gorbi mine.

Correlation of VES-9 and BH-4

The layer parameters of VES-9 are correlated with the lithology of the borehole (BH-4), as shown in Figure 6.12. The surface layer (Topsoil) occurs up to a depth of 2.79 m from the surface. This layer is correlated with geoelectrical layer parameters delineated up to a depth of 1.5 m. Below this layer, a less compact formation occurs at a depth of 2.79 m. It extends up to the depth of 10.04 m in the borehole section, which is correlated with the VES layer showing the resistivity value

of 175 ohm-m, which is indicated as a less compact sandstone. A thick layer of compact sandstone is identified in the borehole section between the depth of 10.4 m and 42.92 m. This is correlated with a high resistivity value of 534 ohm-m, which occurs between the depth of 4.05 m and 35.8 m. The less compact zone obtained in the borehole section at a depth of 2.79 m shows good agreement with VES-9 results. A graph between VES-9 interpreted depth, and borehole depth (BH-4) was plotted as shown in Figure 6.12 (b), and the correlation coefficient was found to be 0.97.

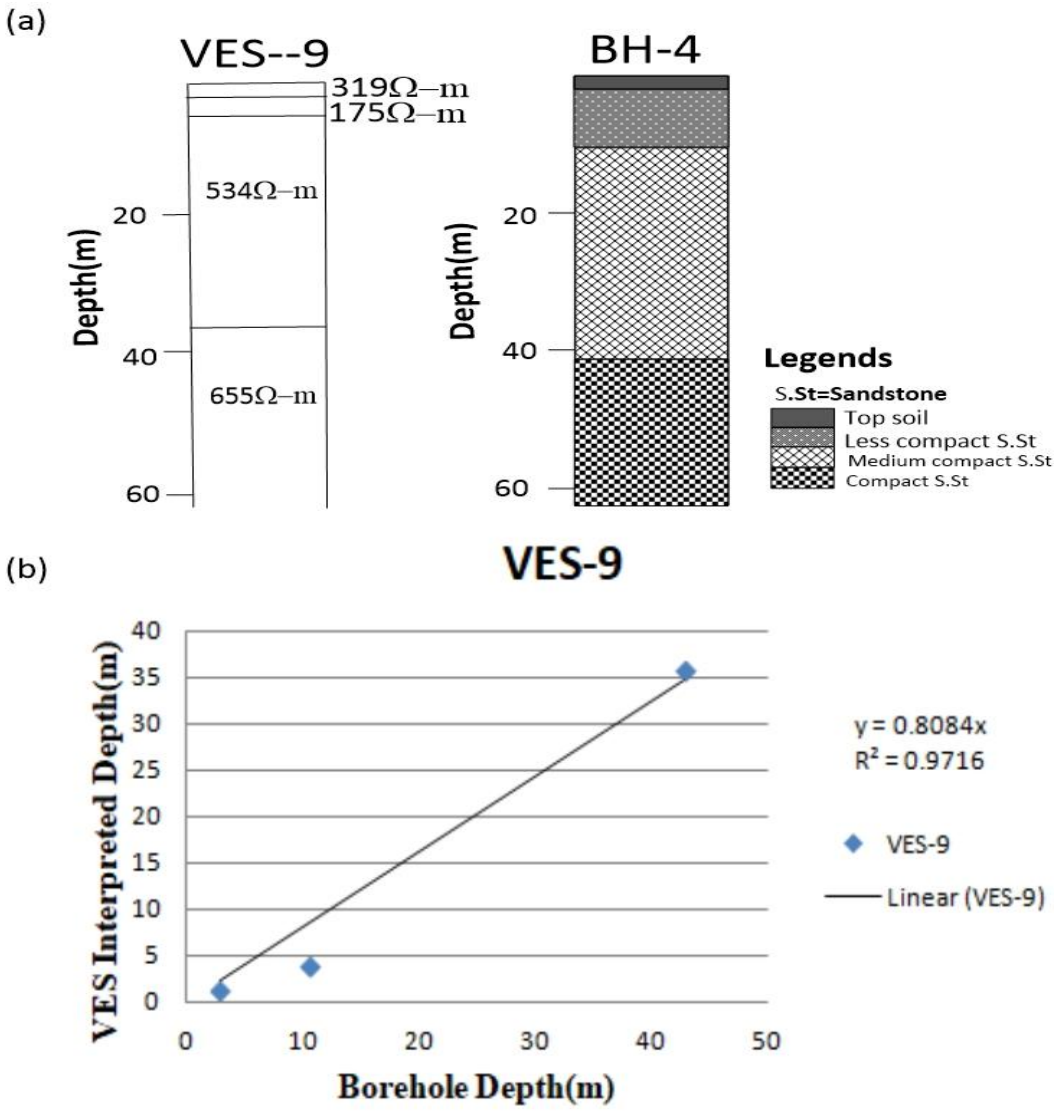

Figure 6.12(a) Lithologic log of borehole BH-4. **(b)** Correlation of VES-9 interpreted depth and borehole (BH-4) depth.

Correlation of VES-10 and BH-11

The borehole (BH-11) near the VES-10 was drilled up to the depth of 62.5 m, as shown in Figure 6.13. The surface layer (Topsoil) with variable nature of soil cover is extended up to a depth of 6.2 m from the ground surface, which is fully correlated with the geoelectrical layers having resistivity values 64.3 ohm-m extending up to a depth of 5.25 m. A weathered formation underlies this layer at a depth of 6.2 m. It extends up to the depth of 32.56 m in the actual borehole section, which is correlated with the VES layer showing a resistivity value of 32.5 ohm-m between the depth of 5.25 and 28.1 m marked as a medium to semi-weathered sandstone. Below this layer, highly weathered sandstone occurring at a depth of 32.56 m and extending up to the depth of 60.7 m in the borehole section is correlated with the VES layer showing a resistivity value of 11.7 ohm-m between the depth of 28.1 and 37.9 m. The highly weathered zone identified in the borehole section at a depth of 32.56 m shows good agreement with the results obtained from VES-10 within the acceptable limit, and the graph of VES-10 interpreted depth versus borehole depth (BH-11) was plotted as shown in Figure 6.13(b). The correlation coefficient was found to be 0.91.

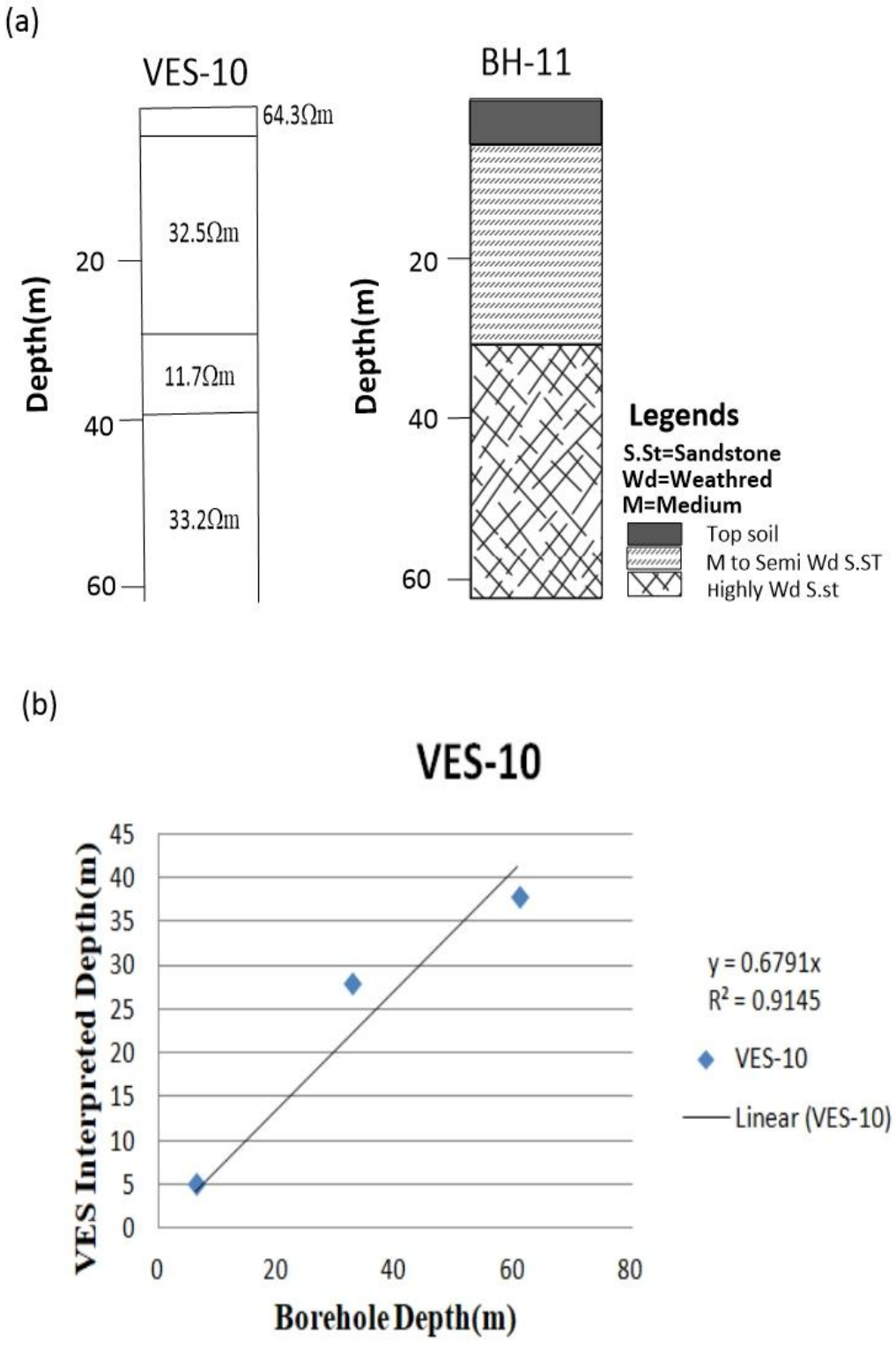

Figure 6.13(a) Lithologic log of borehole BH-11. **(b)** Correlation of VES-10 interpreted depth and borehole (BH-11) depth.

Correlation of VES-40 and BH-8

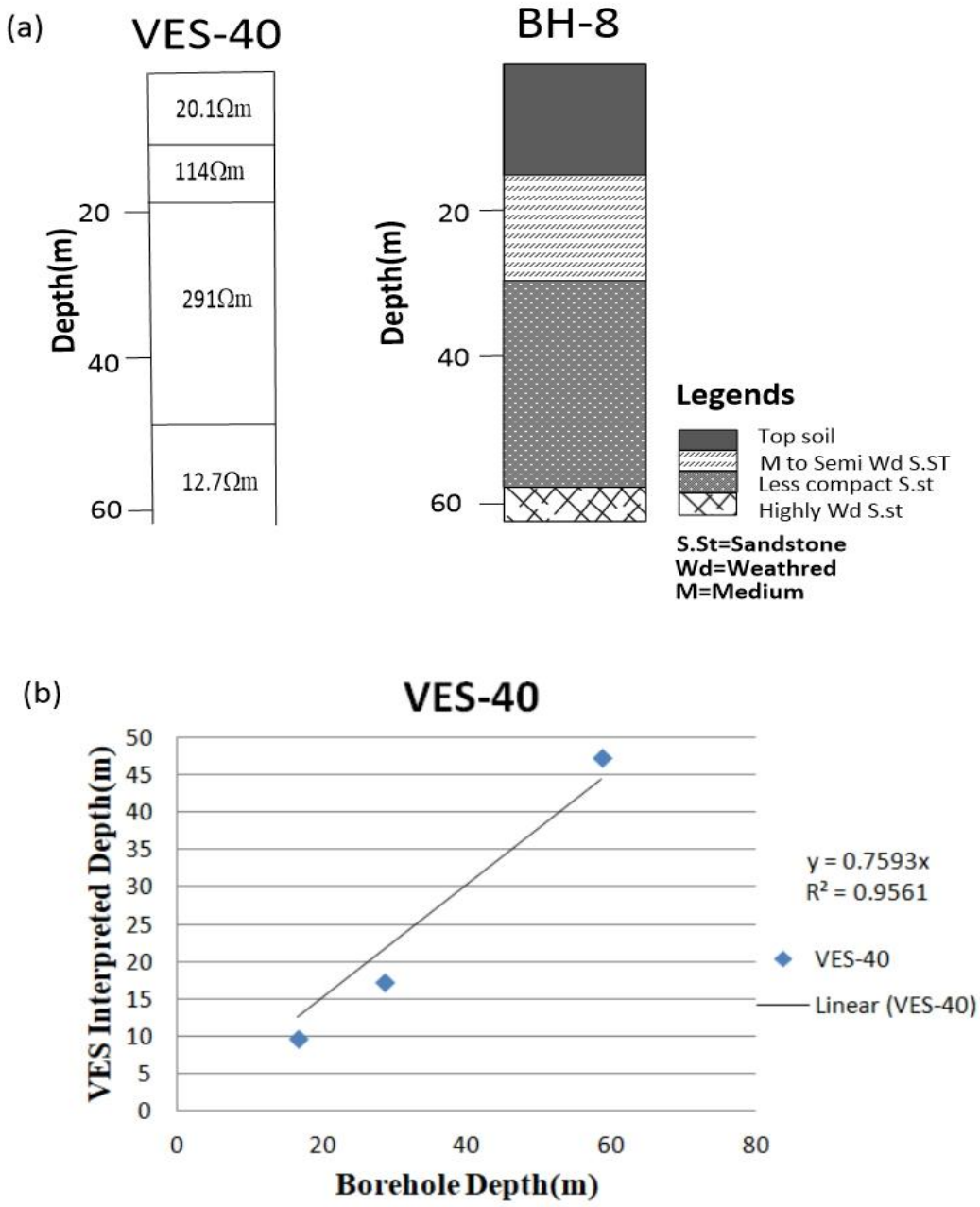

Figure 6.14(a) Lithologic log of borehole BH-8. **(b)** Correlation of VES-40 interpreted depth and borehole (BH-8) depth.

The layer parameter of VES-40 is correlated with the lithology of the borehole (BH-8), as shown in Figure 6.14. The surface layer (Topsoil) occurs up to a depth of 16.5 m from the surface. This layer is correlated with the geoelectrical layer parameter, possesses a resistivity of 20.1ohm-m, and is delineated up to a depth of 9.8

m. Below this layer, a weathered formation occurs at a depth of 16.5 m. It extends up to the depth of 28.5 m in the borehole section, which is correlated with the VES layer having a resistivity value of 114 ohm-m, which may be indicated as weathered to semi-weathered sandstone. A thick layer of less compact sandstone is identified in the actual borehole section between the depth range of 28.5 m and 58.5 m. This is correlated with a resistivity value of 291 ohm-m, which occurs between the depth of 17.3 m and 47.3 m. The weathered zone obtained in the borehole section at a depth of 16.5 m shows good agreement with that obtained from VES-40 results. A graph between VES-40 interpreted depth and borehole depth (BH-8) was plotted as shown in Figure 6.14 (b) and the correlation coefficient was found to be 0.95.

The fifty-five VES data is interpreted using the developed program described in chapter 5 to obtain model parameters (resistivity and thickness). The interpretation of VES data and borehole reveals the following geohydrological formation in the study area.

- Topsoil/Surface soil
- Sand
- Clay
- Highly weathered to semi-weathered sandstone
- Less compact sandstone
- Compact sandstone

Based on the above correlations, the range of resistivity values of the subsurface material has been identified and is presented in Table 6.1. This classification of different lithological units, as shown in the table in collaboration with

the limited borehole logs available in the survey area, has been used for further studies such as geoelectrical cross-sections and other related studies.

Table 6.1 Resistivity ranges for different lithological units

Sr. No.	Lithological Units	Resistivity (ohm-m)
1.	Topsoil	3.83- 953
2.	Clay	< 20
3.	Sand	21- 100
4.	Highly weathered to semi-weathered sandstone	2.28- 120
5.	Less compact sandstone	43.6- 350
6.	Compact sandstone	351-1200
7.	Hard Rock	Very High

6.7.1.2 Vertical geoelectrical cross-section

Five cross-sections have been prepared based on the interpreted results of VES data. Out of five geoelectrical cross-sections, three cross-sections are oriented approximately along the SW-NE direction, and rest two are along the north-south direction.

(i) Vertical geoelectrical cross-section A-A.'

The cross-section A-A' is drawn based on the evaluated geoelectrical layer parameters of the five Vertical Electrical Soundings(VES), i.e., VES-25, VES-16, VES-23, VES-17, and VES-11 with available lithological information from the borehole (BH-13) and it covers a traverse of about 11km approximately in SW-NE direction as shown in Figure 6.15. This section lies south of the Nigahi residential colony and west of the Govind Vallabh Pant Sagar. The surface layer(topsoil) is present all along the section with varying thicknesses. The resistivity of this layer

varies between 13.1 to 87.7 ohm-m due to variations in moisture content and soil type. Below this layer, the weathered sandstone formation is present throughout the section with varying thicknesses. The maximum thickness occurs at the sounding location VES-23 and gradually decreases up to VES-11 in the North-East side and increases up to the sounding location VES-16 and VES-25 in the South-West direction and resistivity of this layer varies from 2.60 to 19.1 ohm-m. Semi-weathered sandstone formations of varying thicknesses underlie this layer. The thickness of this layer increases from NE to SW direction, and the maximum thickness is found below VES-16 and VES-25. Under VES-25, VES-16, and VES-23, a less compact sandstone formation exists, and this layer's resistivity varies from 43.6 to 75.3 ohm-m. Below VES-17 and VES-11, a thick, highly weathered sandstone formation of resistivity 2.8 to 11.9 ohm-m was encountered. Further, this layer is underlain by clay of small thickness. By observing the resistivity cross-section, it is concluded that the aquifer occurring at shallow depths are semi-weathered sandstone layers, and at deeper depths, highly weathered sandstone formation occurring below VES-17 and VES-11 is likely to be a good potential zone for groundwater.

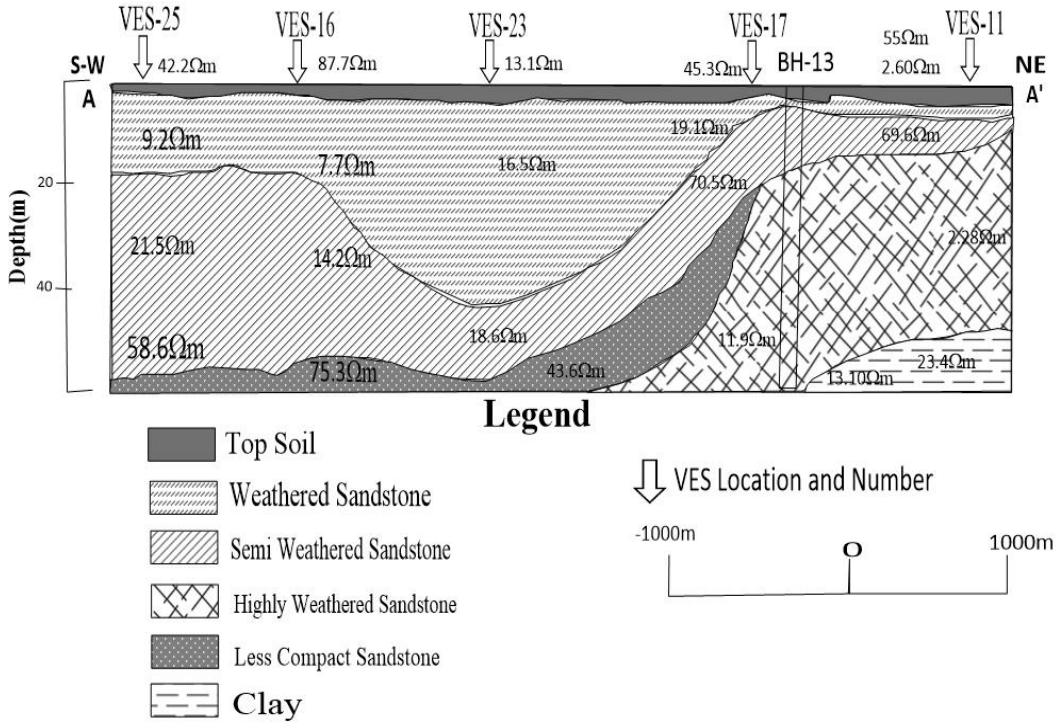

Figure 6.15. Geoelectrical cross-section along profile A-A'.

(ii) Vertical geoelectrical cross-section B-B'

This cross-section lies to the south of the national highway-39 (NH-39) between Nigahi colony and near Ghurital and south of the previous section in Banauli village. The section is oriented approximately in the north-south direction. It covers a traverse of nearly 6.5 km, as shown in Figure 6.16, which incorporates the interpreted results of seven Vertical Electrical Soundings(VES), i.e., VES-24, VES-22, VES-21, VES-19, VES-18, VES-20, and VES-26. The topsoil occurs all along the section with varying thicknesses. The resistivity of this layer varies from 3.83 to 40.1 ohm-m due to variations in moisture content and soil type. Weathered sandstone underlies this layer with a resistivity range between 6.35 to 20.1 ohm-m. Below this layer, the thick semi-weathered layer is present all along the section with a resistivity range varying

from 10.9 to 18.9 ohm-m consisting of weathered sandstone with an average thickness of about 15m. The thickness of this layer increases from VES-24 to VES-22, then gradually decreases from VES-22 to VES-20 in the south direction and again increases at VES-26 in the south direction. This layer is underlain by a less compact formation below VES-24, VES-22, and VES-21. The resistivity of this layer varies from 51.5 to 59.2 ohm-m and is considered a less compact sandstone formation. A thick, highly weathered fourth layer was encountered below VES-21, VES-19, VES-18, VES-20, and VES-26. This layer seems to be saturated with water, and the resistivity of this layer varies from 3.14 to 11.9 ohm-m, considered a highly weathered sandstone formation. The presence of weathered sandstone formations indicates the possibility of the good potential of groundwater resources.

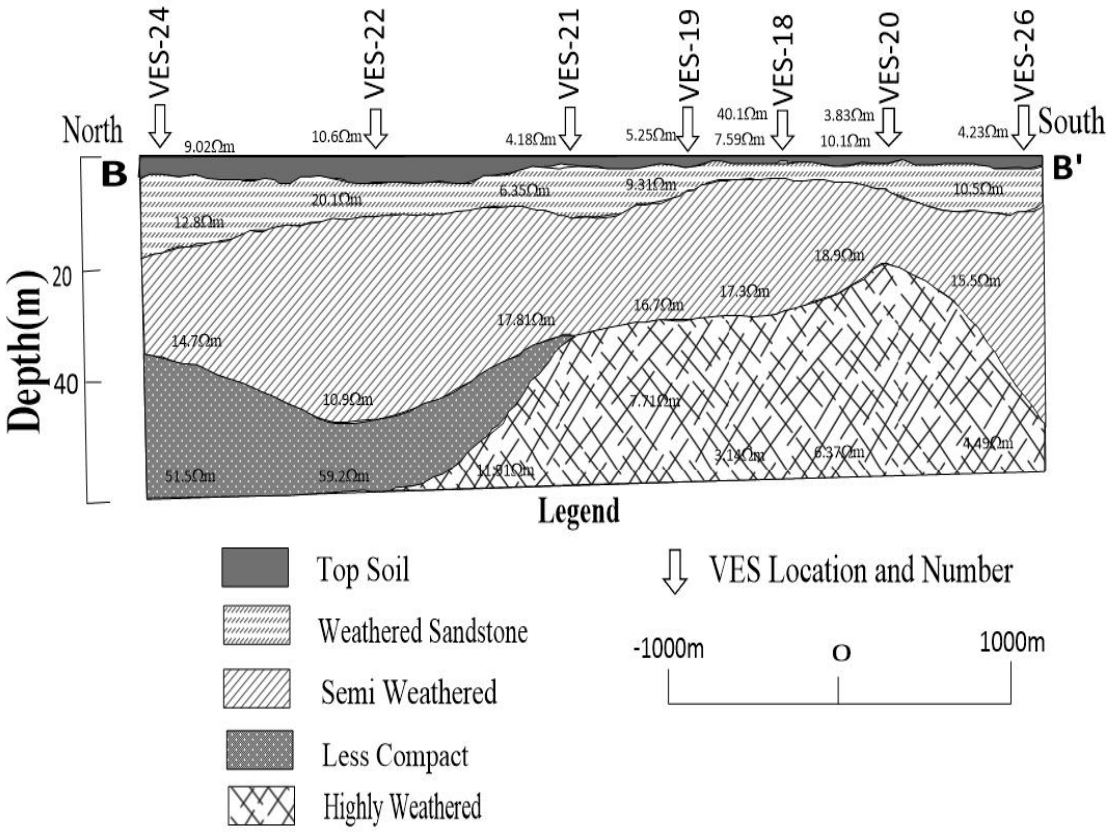

Figure 6.16 Geoelectrical cross-section along profile B-B'.

(iii) Vertical geoelectrical cross-section C-C'

The cross-section C-C' lies west of the Govind Vallabh Pant Sagar and south of the national highway-39 (NH-39) between Dudhichu colony and Waidhan town. This section is oriented in an SW-NE direction, covers a traverse of 5.3km, and incorporates the interpreted results of VES-29, VES-28, VES-27, VES-18, and VES-12, as shown in Figure 6.17. The top layer shows a resistivity variation of 33.2 to 40.1 ohm-m due to moisture content and soil type variation. The thickness of this layer varies from place to place. A thick, highly weathered formation underlies the top layer with a resistivity range between 3.2 to 9.7 ohm-m. Below this layer, the weathered layer is present all along the section, with a resistivity range between 12.8 to 17.3 ohm-m. The thickness of this layer gradually increases below VES-29, VES-28, and VES-27 and decreases below VES-18, again increasing below VES-12 in the NE direction. Below VES-18, a highly weathered zone is identified, having a resistivity of 3.14 ohm-m. The thickness of this layer is maximum below VES-18 and gradually decreases in both SW and NE directions and is considered as highly weathered sandstone formation. Weathered sandstone formation at a different depth within the section indicates the good potential of groundwater resources.

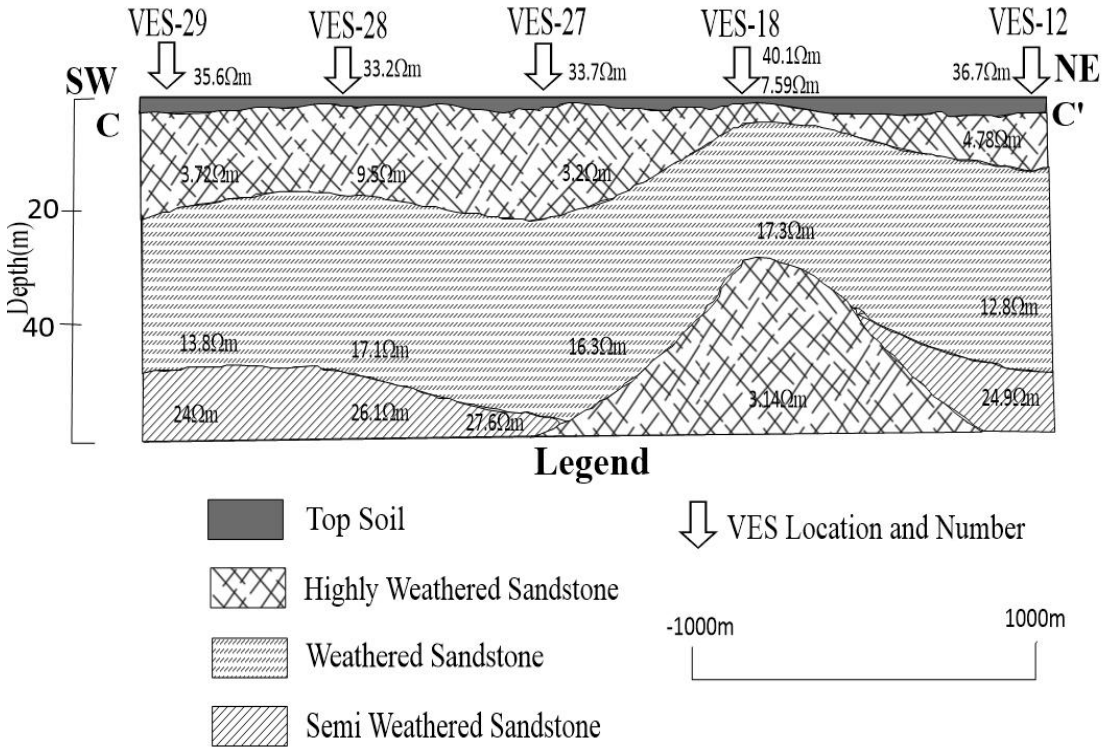

Figure 6.17 Geoelectrical cross-section along profile C-C'.

(iv) Vertical geoelectrical cross-section D-D'

This cross-section lies on the eastern side of the study area between the Kakri residential colony and village Koharauliya. The cross-section D-D' is oriented north-south, covers a traverse of 6.2km and is drawn based on the interpretation results of the five Vertical Electrical sounding(VES) data, i.e., VES-1, VES-2, VES-4, VES-5, and VES-6, as shown in Figure 6.18. The upper layer is present all along the cross-section with approximately uniform thickness and a resistivity range between 7.9 to 92.8 ohm-m. This layer's resistivity varies due to moisture content and soil type variation. Below this layer, weathered to semi-weathered sandstone occurs, having a resistivity range between 9.1 to 51.5 ohm-m. The thickness of this layer increases from north to south and is found to be maximum below VES-5. After VES-5, this

layer's thickness decreases towards the section's south side, i.e., towards VES-6. This layer is underlain by a less compact layer having a resistivity range between 15.8 to 79 ohm-m consisting of less compact sandstone. The thickness of this layer decreases towards the north to the south side of the section; minimum thickness occurs at VES-5 and again increases at VES-6, i.e., at the end of the south side of the section. Below this layer, a more compact formation of resistivity (31.8 to 225 ohm-m) encountered of varying thicknesses from the north to the south side of the section. This layer is underlain by a clayey formation below VES-1 and VES-2 of resistivity 15.2 to 19.4 ohm-m. The existence of weathered to semi-weathered sandstone formations within the cross-section indicates the presence of good groundwater sources.

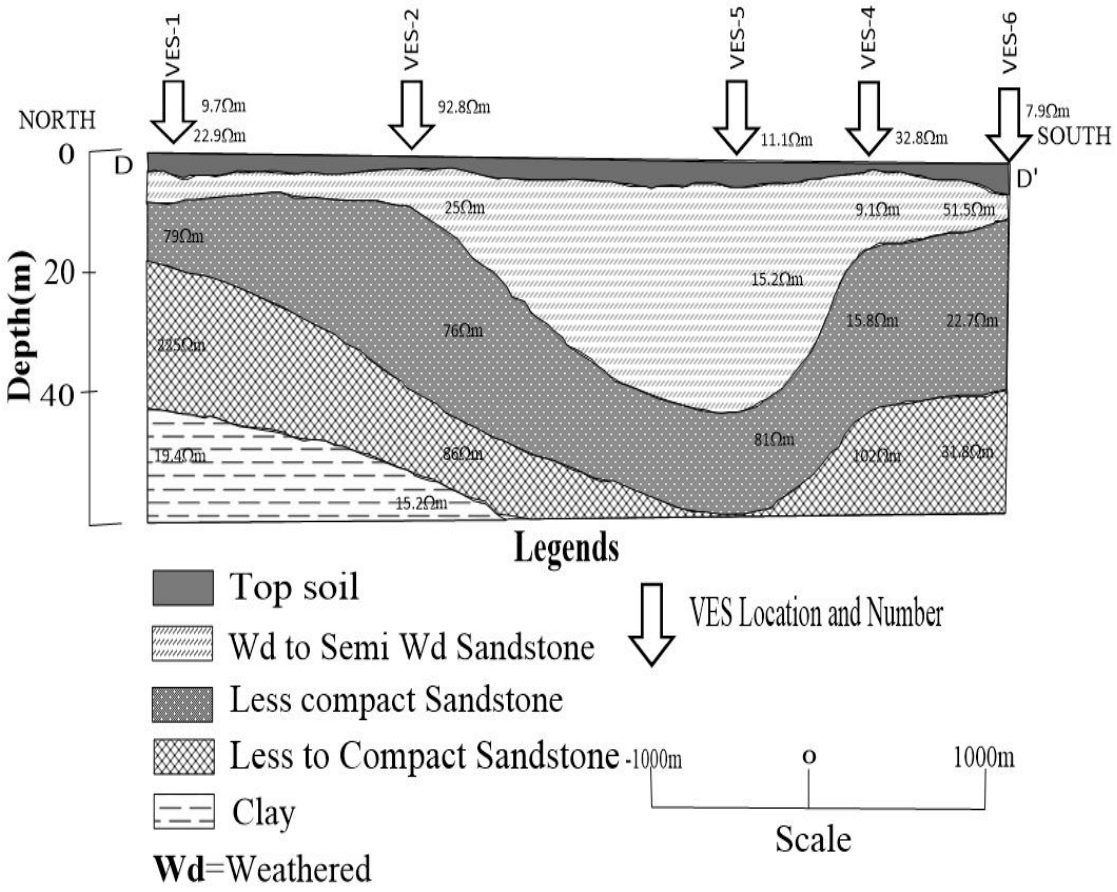

Figure 6.18 Geoelectrical cross-section along profile D-D'

(v) Vertical geoelectrical cross-section E-E'

The cross-section E-E' shown in Figure 6.19, covers the northern part of the study area oriented in SW-NE direction and covers a traverse of 5km. This is built-in with the interpretation results of six VES sounding, i.e., VES-33, VES-38, VES-40, VES-41, VES-42, and VES-43. The top layer is present all along the section having resistivity variation in the range 9.97 to 53.1 ohm-m. The resistivity of this layer varies due to variations in soil type and moisture content. A thin weathered sandstone formation underlies this layer with a resistivity range between 8.95 to 23.2 ohm-m below VES-33, VES-43, VES-41, and VES-42 along the section. Below VES-42, VES-40, and VES-38, a thin, less compact sandstone formation was found. This layer is underlain by highly weathered sandstone of varying resistivity (3.86 to 29.74 ohm-m) throughout the section. The thickness of this layer varies from the SW-NE direction. The maximum thickness of this layer occurs at VES-43(left side) and VES-40(right side) of the section, and the minimum thickness occurs at VES-41 and VES-42 in the central portion of the section. Below VES-33, VES-41, and VES-42, a layer of semi-weathered sandstone is identified, having a resistivity range between 26.1 to 55.5 ohm-m. This layer is absent below VES-43 and VES-38, and the thickness of this layer is highly variable maximum occurs below VES-41 and VES-42. Below VES-43, a thick weathered sandstone layer is identified having a resistivity of 11.29 ohm-m. In the north-eastern side below VES-38, a thick compact hard rock of resistivity 5989 ohm-m was identified. The occurrence of highly weathered sandstone formation in the section facilitates the presence of good groundwater sources.

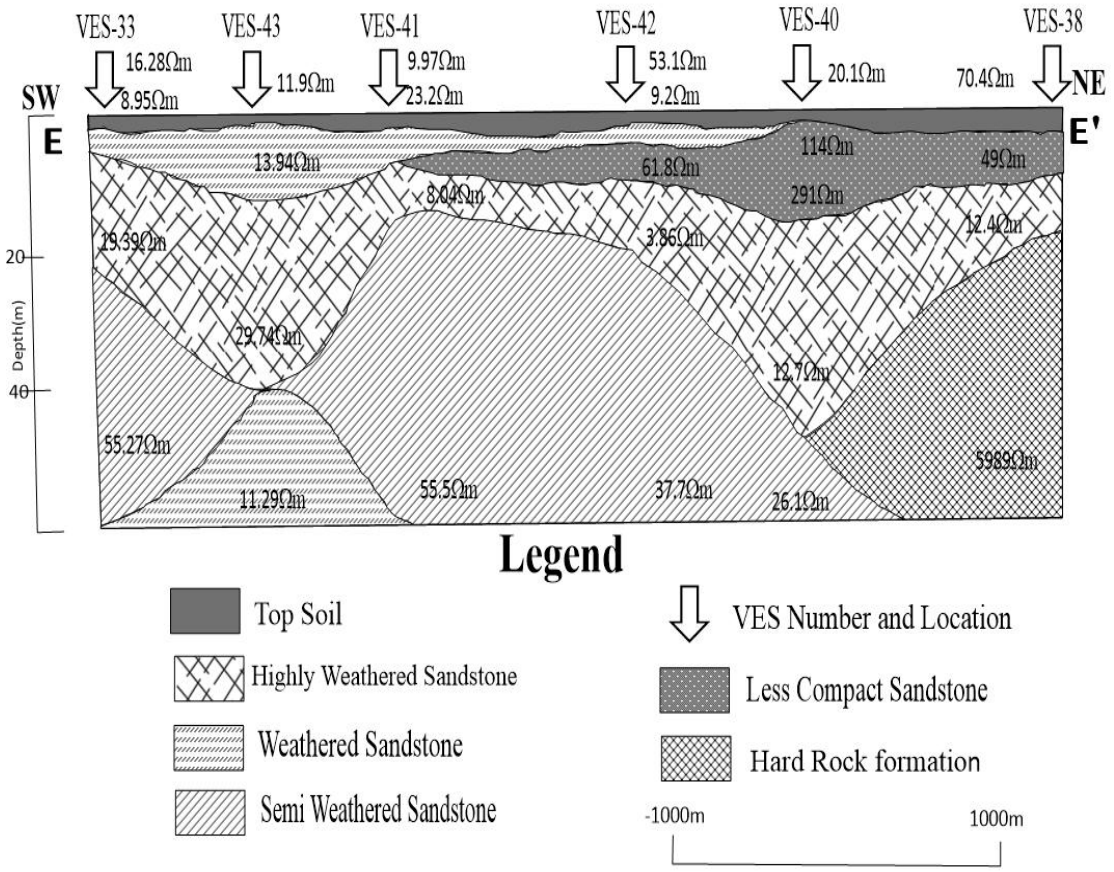

Figure 6.19 Geoelectrical cross-section along profile E-E'.

6.7.1.3 Characterization of aquifers using VES data

In this study, the resistivity interpretation provided geoelectric properties that were used to determine secondary parameters called Dar-Zarrouk parameters. These parameters were calculated using the resistivity (ρi) and thickness (hi) values of the geoelectrical layers obtained from electrical sounding conducted in the study areas. The purpose of determining the Dar-Zarrouk parameters was to better understand the geoelectrical models, which comprise stratified layered formations. These parameters help to evaluate important characteristics of aquifers, such as transmissivity and the protective capacity of the overlying rock materials (Salem, 1999).

However, in the present work, the correlation between Dar-Zarrouk parameters and hydraulic parameters has not been attempted due to the unavailability of pumping test data of the study areas.

6.7.1.3.1 Iso-Resistivity map analysis

Iso-apparent resistivity maps describe the spatial distribution of apparent resistivity within aquifer layers and the degree of weathering across a particular horizontal plane at a predetermined depth. These contour maps of apparent resistivity have proven valuable in identifying aquifers, as regions with lower resistivity values on the contour maps and indicate possible groundwater potential zones (Ishola et al., 2013). To create these maps, iso-apparent resistivity contour lines were generated at different depths corresponding to half of the current electrode distances AB/2, specifically at 6m, 25m, 50m, 100m, 160m, and 200m. The apparent resistivity values at different AB/2 distances are given in Table 6.2.

Table 6.2 Apparent resistivity(ohm-m) at half the current electrode distance(AB/2).

VES No.	AB/2=6m	AB/2=25m	AB/2=50m	AB/2=100m	AB/2=160m	AB/2=200m
30	30.8	66	118.7	200.76	273.12	315
31	114.23	272.47	506.13	799.45	957.67	1052.13
32	16.59	15.65	18.86	23.69	26.73	28.58
33	11.1	17.73	25.87	35.42	39.12	41.45
34	15.7	18.1	26.82	37.09	41.47	44.58
35	46.21	101.04	177.95	294.31	352.12	405.12
36	67.12	105.38	98.82	28.77	24.42	23.02
37	51.21	101.33	128.58	136.78	119.17	115.23
38	47.77	26.7	45.21	95.32	120.1	135.21
39	179.12	134.54	143.23	318.3	356.7	410.12
40	68	106.26	99.7	29.65	25.3	23.9
41	13.9	12.11	25.43	34.47	37.87	39.23
42	16.1	17.2	12.6	15.4	20.1	25.2
43	13.69	16.9	21.18	22.63	29.87	34.67
44	20.2	35.12	69.1	107	168	210
45	100.45	77.26	123.71	212.42	315.76	377.67
46	110.86	186.49	226.42	347.67	419.86	457.35
47	86.48	91.88	115.47	226.33	330.67	399.58
48	31.47	49.29	79.39	159.2	215.7	255.5
49	75.02	78.59	103.19	193.94	259.67	303.2
50	87.91	64.72	111.17	199.88	303.22	365.13
51	93.75	70.56	117.01	205.72	309.06	370.97
52	14.33	29.16	63.27	101.08	112.57	121.22
53	45.46	49.03	73.63	164.38	230.11	273.64
54	12.86	19.49	27.63	37.18	40.88	43.21
55	21.97	21.036	24.24	29.06	32.1	33.95
Minimum	11.1	12.11	12.6	15.4	20.1	23.02
Maximum	179.12	272.47	506.13	799.45	957.67	1052.13
Average	53.55	68.616	99.358	155.996	198.513	227.11

Iso-apparent resistivity contour map and 3D surface maps were constructed for depths corresponding to half of the current electrode distance AB/2=6, 25,50,100,160, and 200m using SURFER Version 20 software as shown in Figure 6.20(a-f), respectively. The aim was to investigate the changes in apparent resistivity vertically and horizontally at various depths in the subsurface, as well as the variations in weathering intensity within the basement areas and transitional zones.

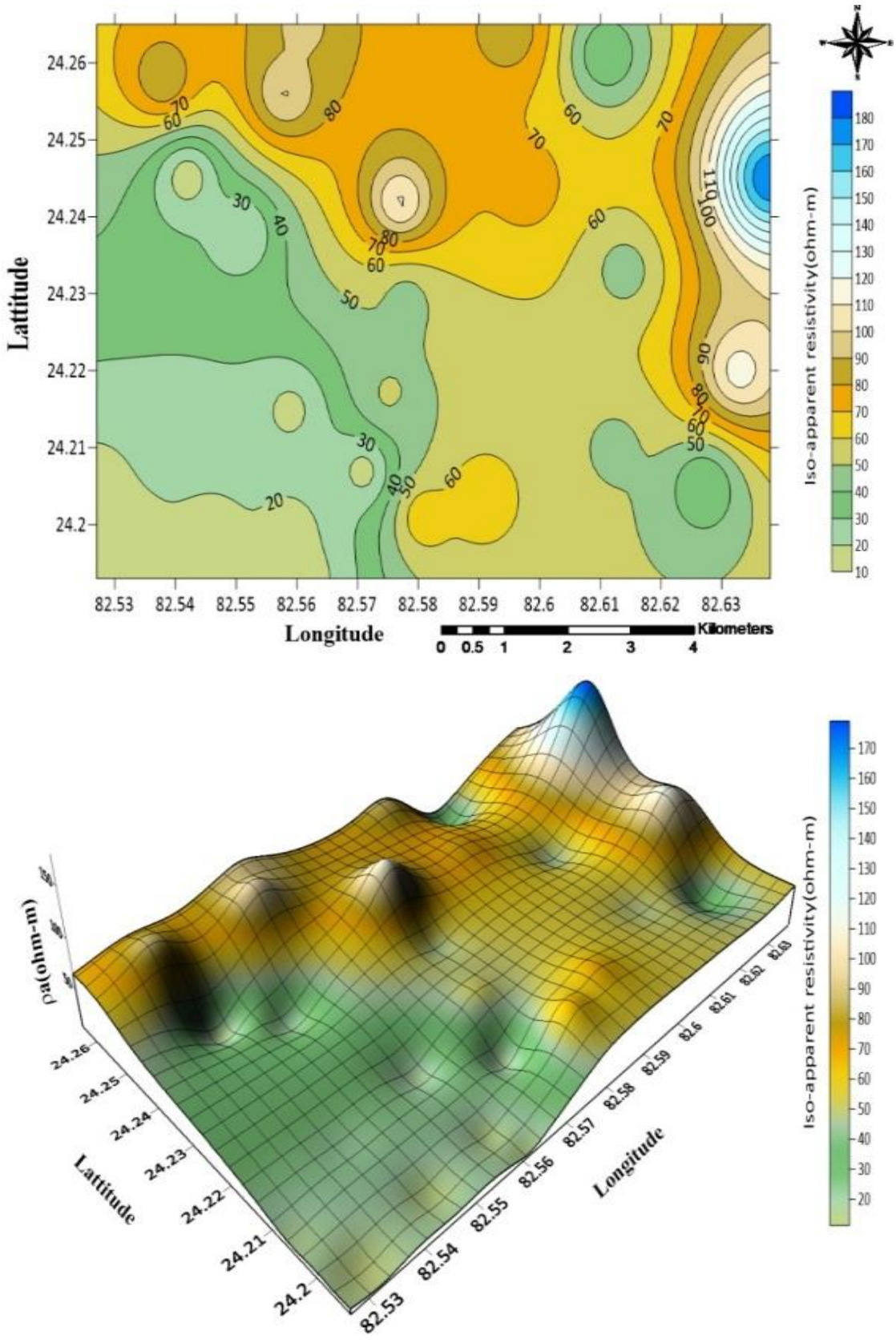
Lattitude
Longitude
Kilometers
0 0.5 1 2 3 4
Iso-apparent resistivity(ohm-m)
Pa(ohm-m)

(a)

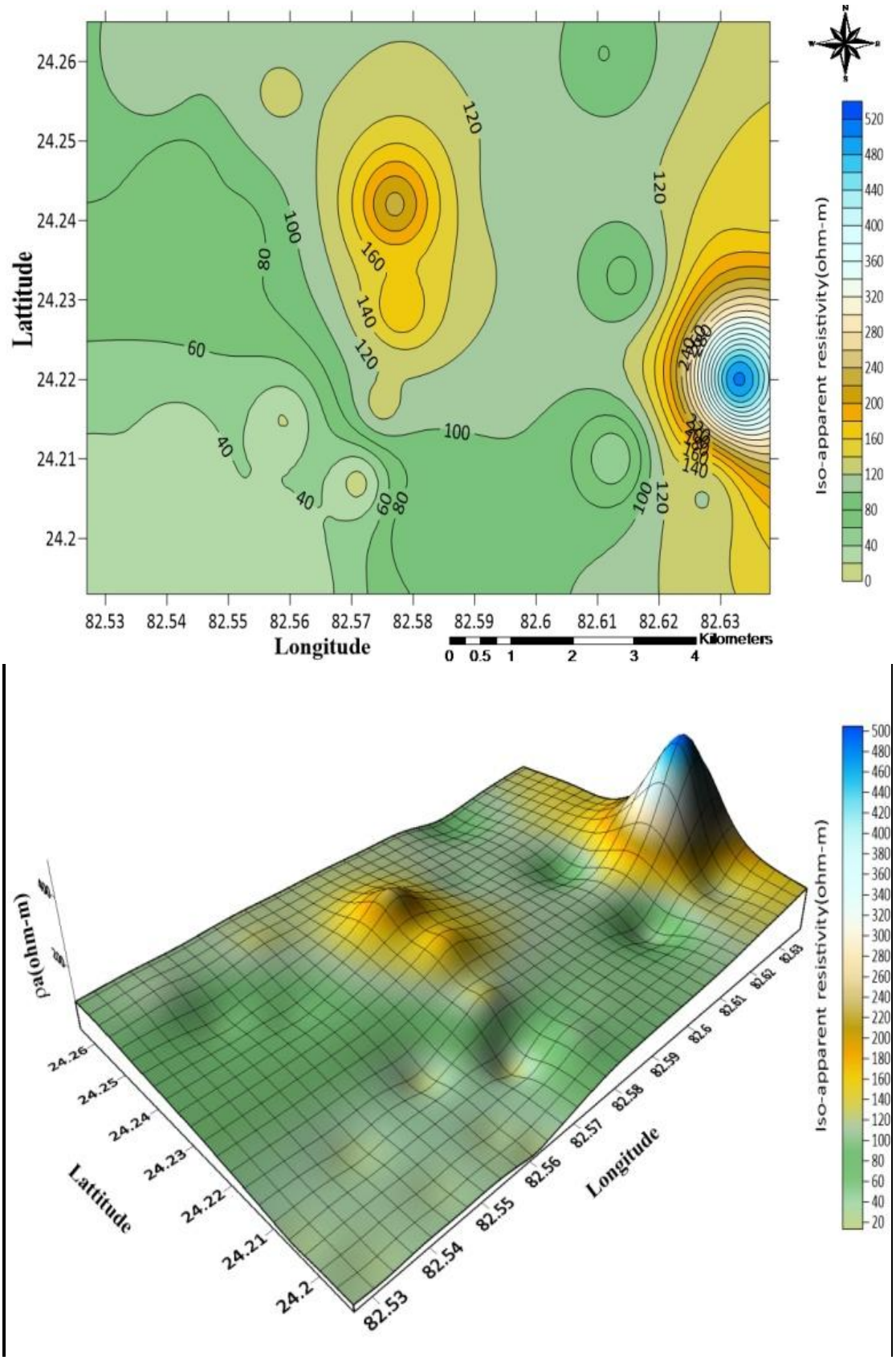
Lattitude
Longitude
Kilometers
0 0.5 1 2 3 4
Iso-apparent resistivity(ohm-m)
ρa(ohm-m)

(b)

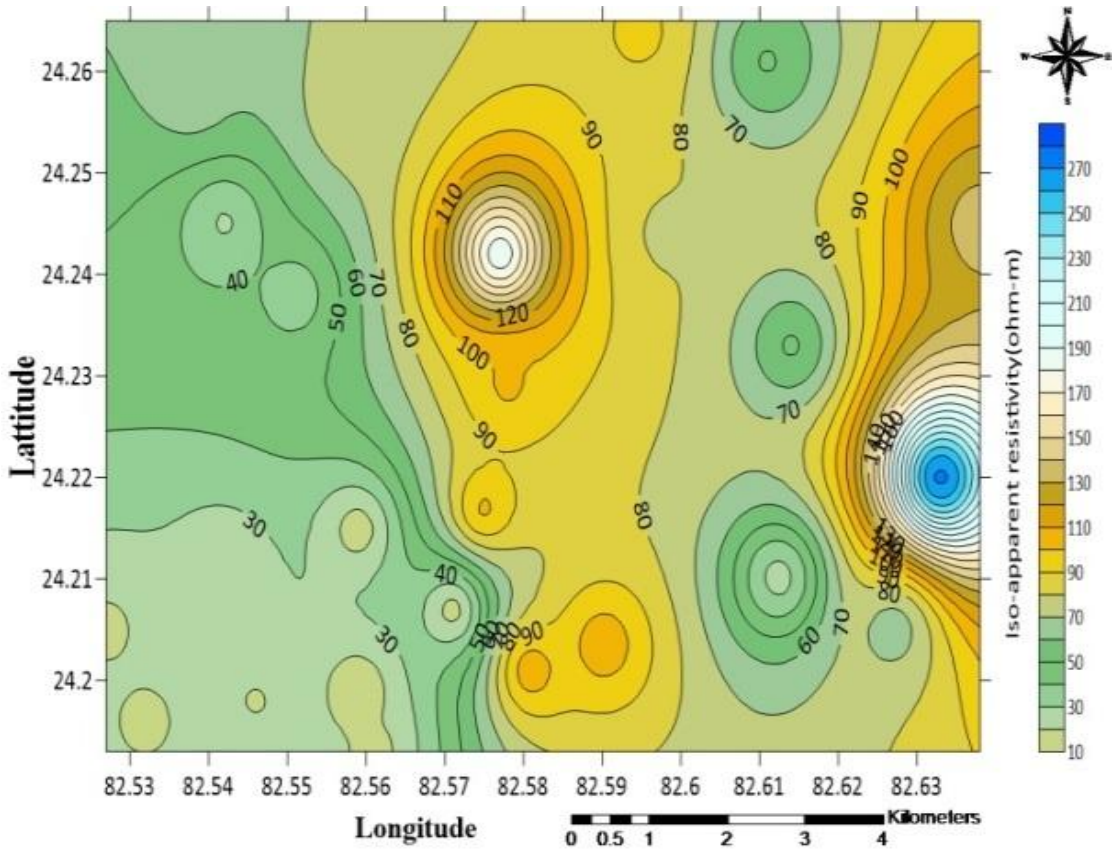
Lattitude
Longitude
Kilometers
0 0.5 1 2 3 4
Iso-apparent resistivity(ohm-m)

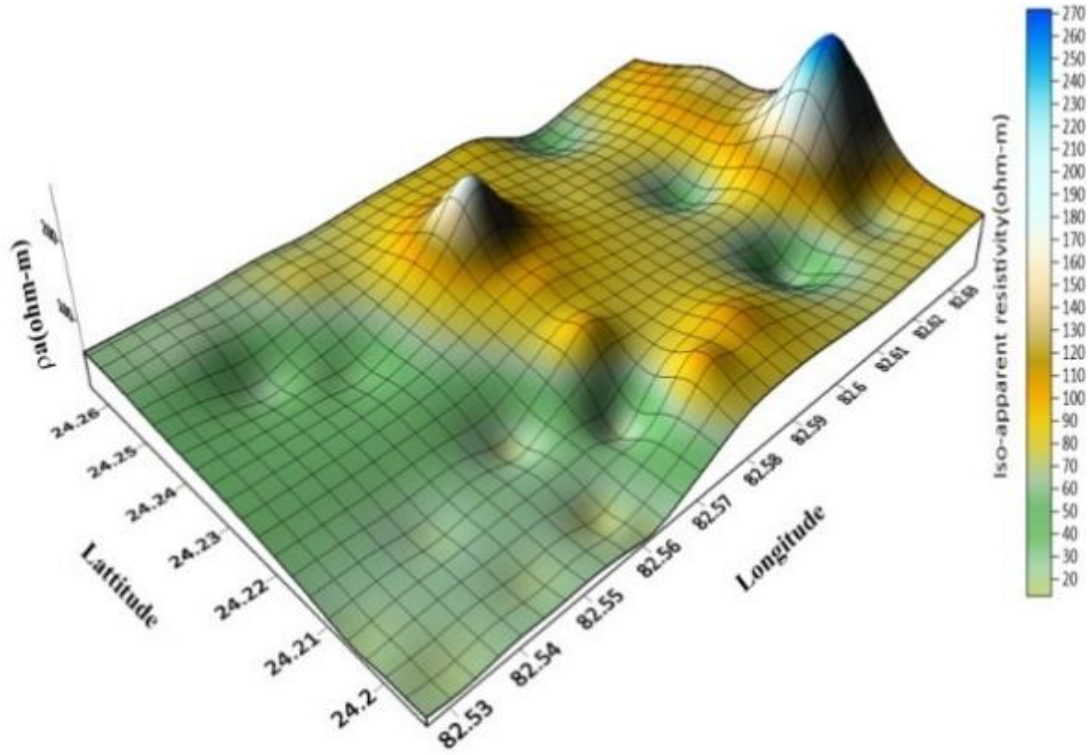
ρa(ohm-m)
Lattitude
Longitude
Iso-apparent resistivity(ohm-m)

(c)

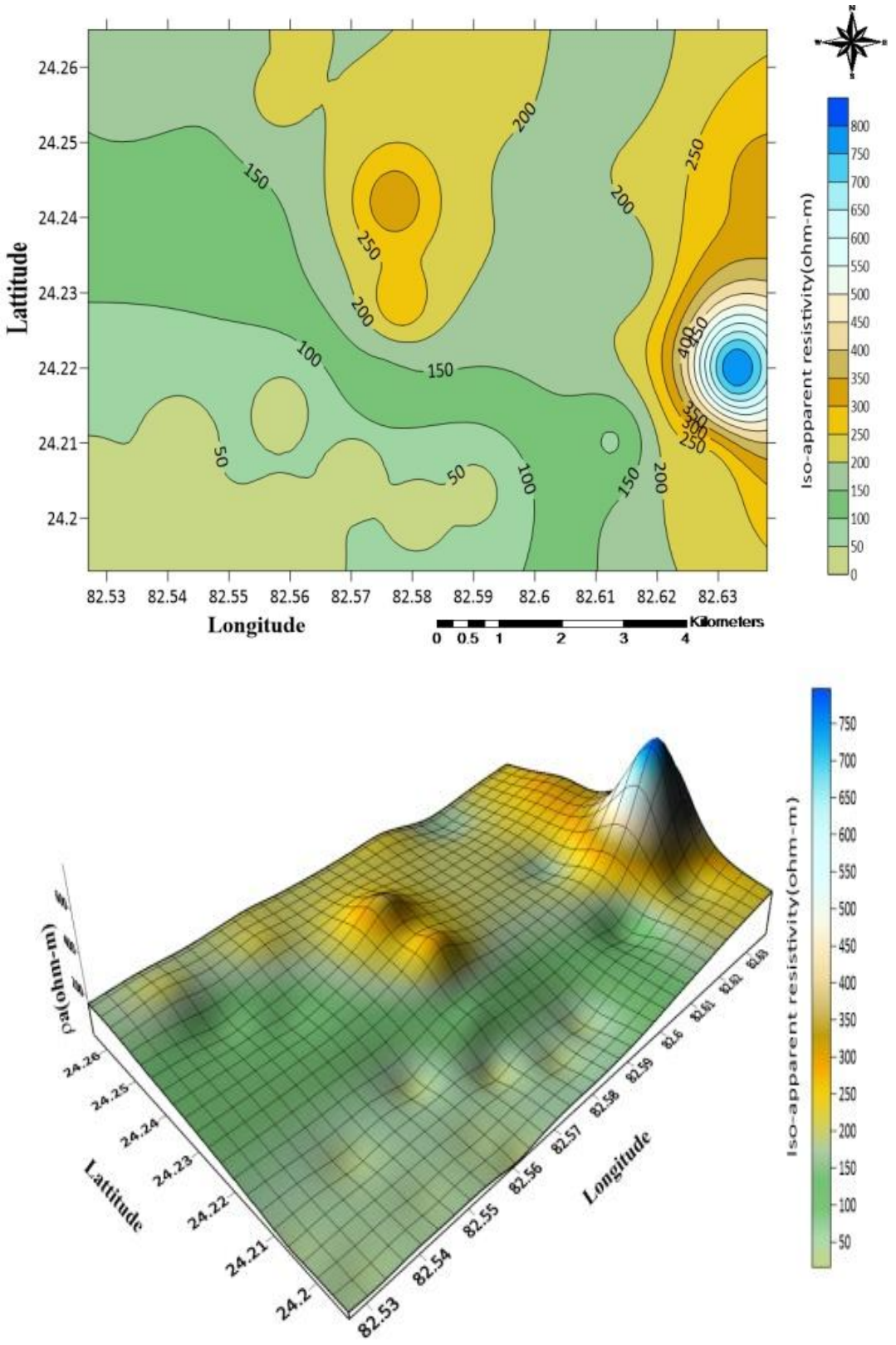
Lattitude
Longitude
Kilometers
Iso-apparent resistivity(ohm-m)
ρa(ohm-m)

(d)

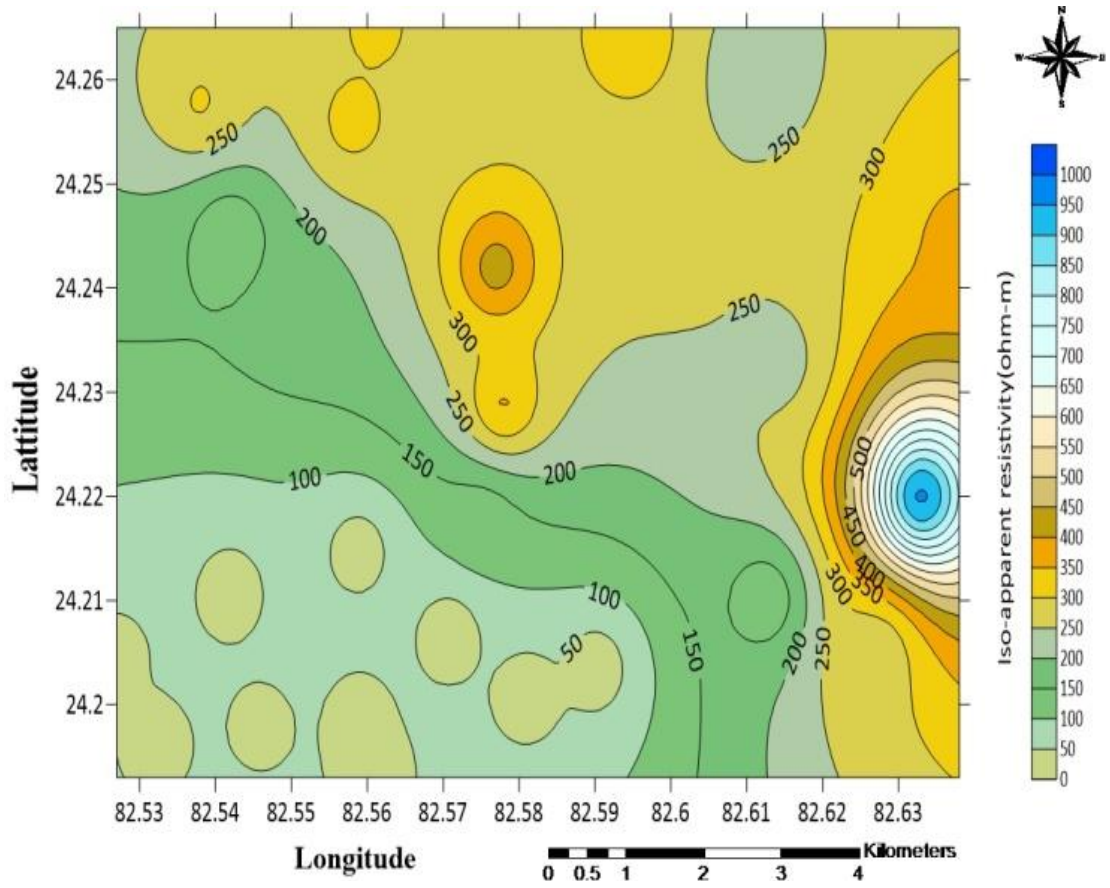
Lattitude
Longitude
Kilometers
0 0.5 1 2 3 4
Iso-apparent resistivity(ohm-m)
ρa(ohm-m)

(e)

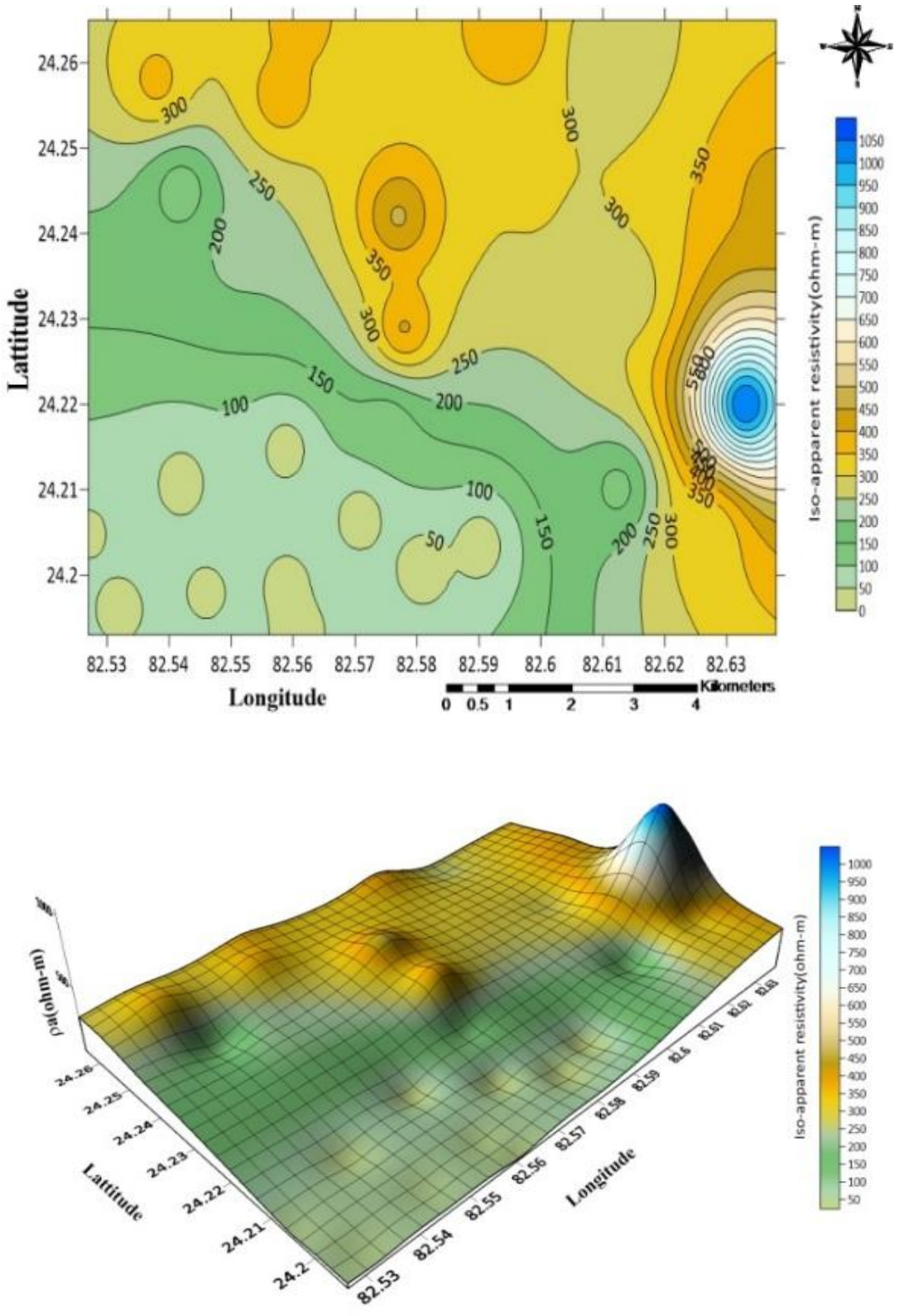

(f)

Figure 6.20(a-f) Iso-apparent resistivity Contour maps and 3D Surface maps

As shown in Figure 6.20(a-f), the iso-apparent resistivity map revealed a progressive increase in resistivity with depth, suggesting a less resistive overburden to the resistive layer at the base. The central axis, western, southern, and south-western portions of the study area have lower apparent variation with depth than the rest portion of the study areas. The higher resistivity zone (>500 ohm-m) occurs on the eastern side of the study area at AB/2=50,100,160, and 200m. This scenario occurs because of the gradual decrease in the sandstone's porosity and permeability with increasing burial depth in these regions.

6.7.1.3.2 Overburden thickness (H) and Dar-Zarrouk parameters map analysis

In order to characterize the aquifers, to delineate the depth of the aquifer and its lateral extent, and estimate the aquifer protective capacity in the study area, 2-D and 3-D spatial contour maps for longitudinal conductance (S), transverse resistance (T), total longitudinal resistivity (ρ_l), total transverse resistivity (ρ_t), coefficient of anisotropy (λ) and overburden thickness(H) are prepared using SURFER Version 20 software. These contour maps are used to understand parameters' spatial variation and delineate potential groundwater potential zones (Gupta et al. 2015.) The estimated Dar-Zarrouk parameters are shown in Table 6.3

Table 6.3 Overburden thickness (H) and Dar-Zarrouk parameters (S, T, ρ_l,ρ_t,λ)

VES No.	Location	H (m)	S (mho)	T (ohm-m^2)	ρ_l=H/S (ohm-m)	ρ_t=T/H (ohm-m)	λ
30	Singrauli village	62.1	0.461085	25561.74	134.6822	411.6222	1.748213
31	Khatas	72.3	0.102114	235808.6	708.0293	3261.53	2.146273
32	Mahdahiya	96.8	4.467544	2223.19	21.66739	22.96684	1.02955
33	Padri	22.4	1.38239	393.97	16.20383	17.58795	1.041835
34	Rampurua	60	2.149513	2076.14	27.9133	34.60233	1.113389
35	Inurra	46.1	0.331427	8436.44	139.0956	183.003	1.147024
36	Naudiya	40.6	4.313904	3797.46	9.411428	93.5335	3.152505
37	Phulzar	64.6	0.48181	13099.45	134.0779	202.7779	1.229792
38	Gorbi Basti	22.1	1.294338	599.56	17.07436	27.12941	1.260515
39	Khirwa	27.5	0.319413	8954	86.09547	325.6	1.944697
40	Gorbi block -b colony	47.6	2.54375	3680.38	18.71253	77.31891	2.032716
41	Rajkhand	14.8	1.891764	146.89	7.823386	9.925	1.126336
42	Naudia	21.2	3.878892	387.06	5.465478	18.25755	1.827709
43	solang	84.21	5.733802	1487.63	14.68659	17.66572	1.096744
44	Kasar	90.5	0.966378	16940.6	93.64868	187.189	1.413804
45	Barhati	119.4	0.535974	51812.3	222.7722	433.9389	1.395673
46	Lotan	38.4	0.213055	7358.45	180.2355	191.6263	1.031116
47	Barwani	76.8	0.388053	85966.46	197.911	1119.355	2.378203
48	Piparkhad	55.8	0.603963	147089.2	92.3898	2636.007	5.341476
49	Karaila	63	0.491485	10435.48	128.1829	165.6425	1.136766
50	Bhaudar	85	0.496115	50672.02	171.3311	596.1414	1.865334
51	Pipra	72.3	0.463697	27896.76	155.9209	385.8473	1.573097
52	Gangi	22	0.821613	795.26	26.77658	36.14818	1.161892
53	Tikuritola	62.9	0.646813	15049.94	97.24596	239.2677	1.568579
54	Thurua	64	2.274459	2022.12	28.13856	31.59563	1.05965
55	Ramgarh	93.9	3.406706	2698.25	27.56328	28.73536	1.02104
Minimum		14.8	0.102114	146.89	5.465478	9.925	1.02104
Maximum		119.4	5.733802	235808.6	708.0293	3261.53	5.341476
Average		58.70423	1.5638483	27899.59	106.2714	413.6544	1.64784338

The 2D and 3D spatial contour maps of overburden and Dar-Zarrouk parameters are described below:

Overburden Isopach Map

The depths to the basement (overburden thickness) beneath the sounding points were plotted as shown in Figure 6.21 (a) and (b). This was evaluated to know a general view of the aquifer geometry of the study area. The overburden is assumed to include the topsoil, clay/pebbles of various degrees of saturation, fine sands, and fractured/weathered rock. The thickness value ranges from 14.8 to 119.4 m. The map of the overburden thickness shows that most of the survey area has a thickness value between 15 to 90 m. Areas with a thickness of less than 50 m are observed to occupy the central axis, southern, north-eastern, north-western, and south-western flank of the map and are observed as a depressed surface in the 3-D map. Areas with thick overburden greater than 100 m are observed across the northern part and occur as an elevated surface in a 3-D map. A portion with a thickness between 55 to 90m is observed in the central axis, northern, western, and south-eastern parts and occurs as a slightly elevated surface in the 3-D map. The existence of a substantial layer of sediment covering the underlying rock formation enhances the availability of groundwater resources in the region, particularly when the rock underneath is weathered. Regions characterized by a significant thickness of sediment in concurrence with basement depressions exhibit a high potential for groundwater, especially within the basement complex area (Wright, 1990; Meju et al., 1999).

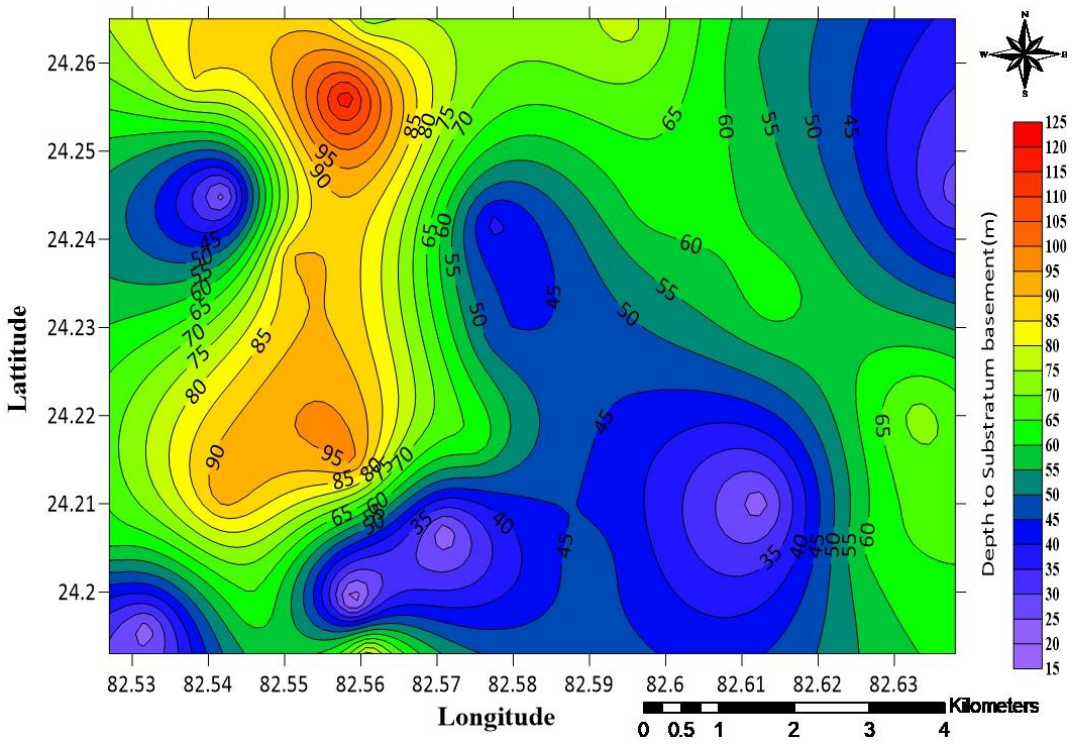

(a)

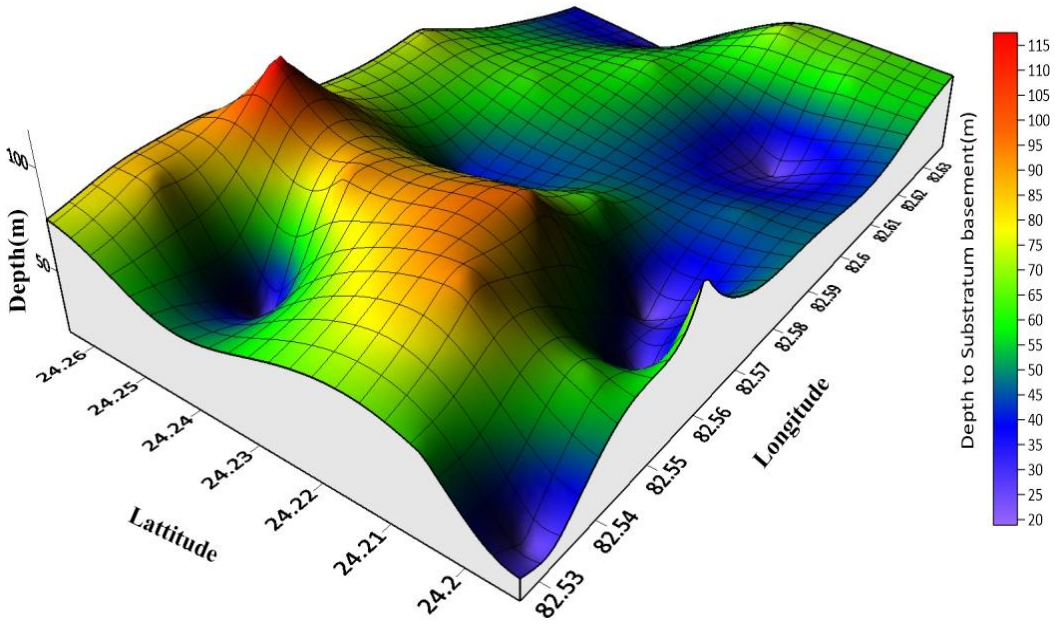

(b)

Figure 6.21. Overburden Isopach Map (a) 2D Contour map of the overburden thickness,(b) 3D Surface map of overburden thickness.

Total Transverse Resistance (T) Map

Total transverse resistance (T) is one of the important parameter to evaluate the potential of groundwater in the study area. Aquifer transmissivity, which represents the ability of a layer to transmit fluids through its entire thickness. Empirically, it can be inferred that the transmissivity of an aquifer is directly related to its total transverse resistance (Henriet, 1976; Ward, 1990) and it is calculated using Equation (6.29). The contour map of total transverse resistance for the study area is shown in Figure 6.22 (a), while the three-dimensional surface map is presented in Figure 6.22 (b). These maps are prepared based on the computed values of total transverse resistance(T) given in Table 6.3.

The total transverse resistance of the study area ranges from 146.89 to 235808.6 ohm-m^2 and is classified as the good, moderate, and low potential zones. Values of T that range between 20,000 to 40,000 ohm-m^2 and those above 40,000 ohm-m^2 are considered moderate and good potential zones, respectively. The 70% of the study area was observed to have T in the range of 10000 to 80000 ohm-m^2. The central axis, western and south-western part of the study area have T less than 20000 ohm-m^2 and falls in poor groundwater potential zones. In 3D maps, these are observed as flat and depressed surfaces. The northern, eastern, north-western, south-eastern, and some central parts of the study area exhibit T greater than 20000 ohm-m^2. In 3D maps, these are observed as sharp peaks surfaces, hence highly permeable to fluid movement. So moderate to good groundwater potential zones are observed in these regions.

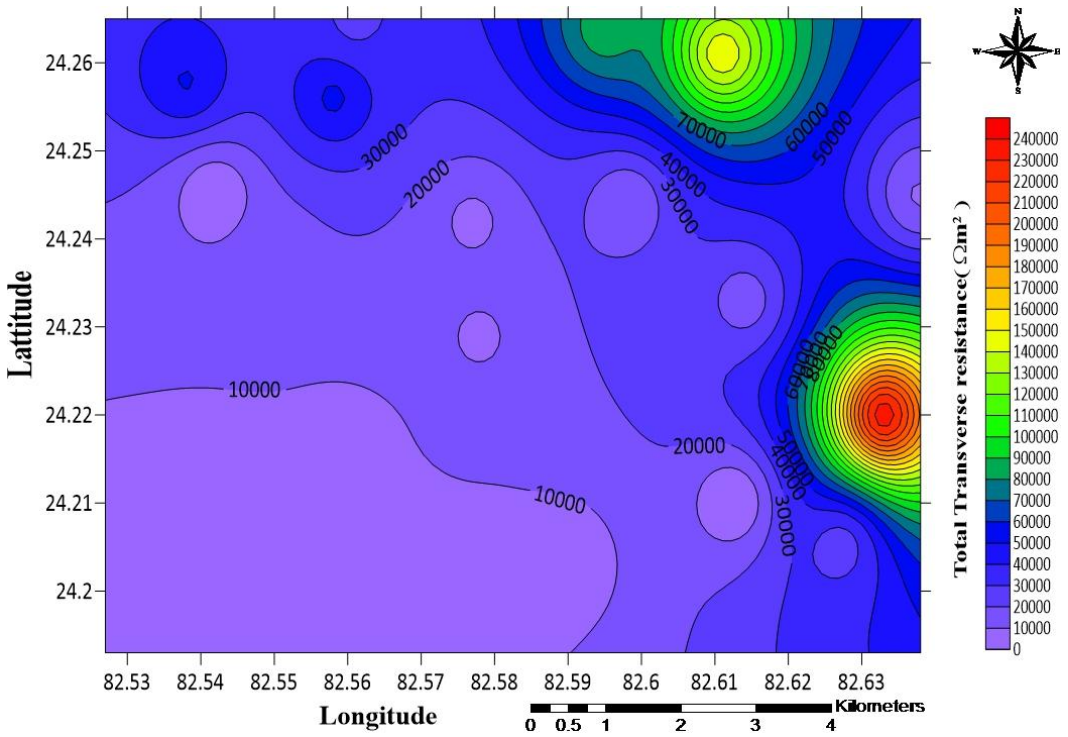

(a)

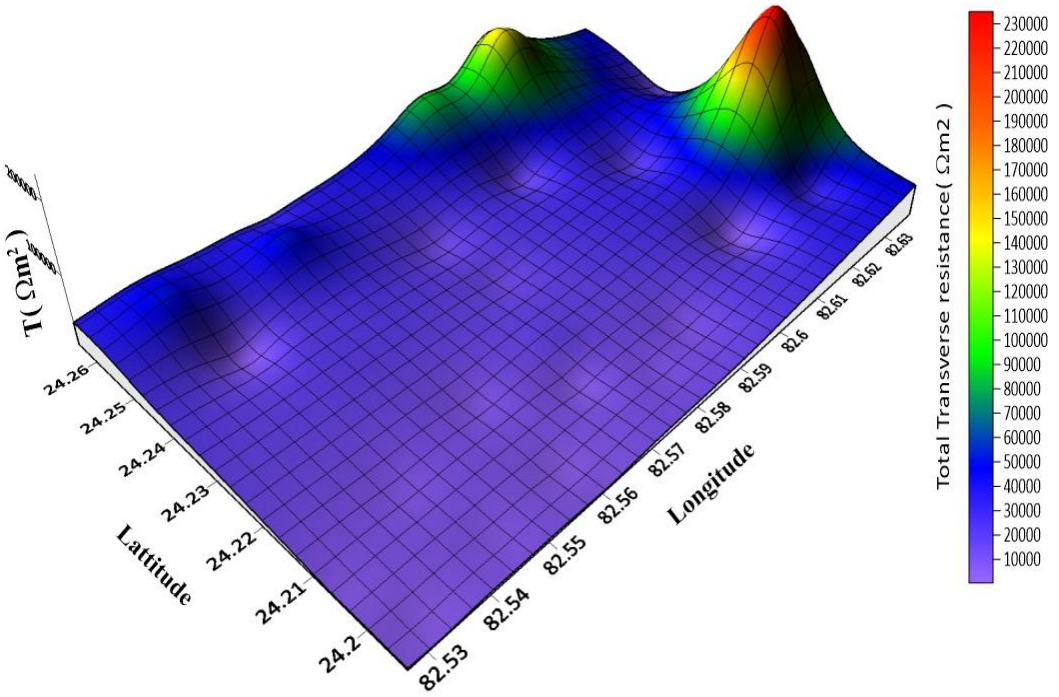

(b)

Figure 6.22 Total Transverse resistance **(T)** Map (a) 2D contour map of **T**,(b) 3D surface map **T**.

Total Longitudinal Conductance(S) Map

The longitudinal conductance, which constitutes the Dar-Zarrouk parameters, has been calculated from the primary parameters using equations (6.28). Contour maps showing the spatial distribution of longitudinal conductance in the area are presented in Figure 6.23. The longitudinal conductance map serves two purposes: firstly, it is used in conjunction with the transverse resistance map to identify groundwater potential zones; secondly, it illustrates the protective capacity of the overlying layer of the aquifers.

In the study area, the values of longitudinal conductance range from 0.102 to 5.77 mhos. The map is categorized into good, moderate, and poor groundwater potential zones based on the observed values of S. Regions with a longitudinal conductance (S) lower than 2 mhos, between 2 to 4 mhos, and greater than 4 mhos are categorized as good, moderate and poor groundwater potential zones respectively (Ndatuwong and Yadav, 2015). The areas identified as good groundwater potential zones are further compared to the transverse resistance map. It has been observed that the regions surrounding the northern, eastern, north-western, south-eastern, and certain central parts of the study area exhibit a total transverse resistance exceeding 20,000 ohm-m^2 and a total longitudinal conductance below 0.8 mhos. These areas are observed to possess favorable groundwater potential due to their low S values and high T values.

.

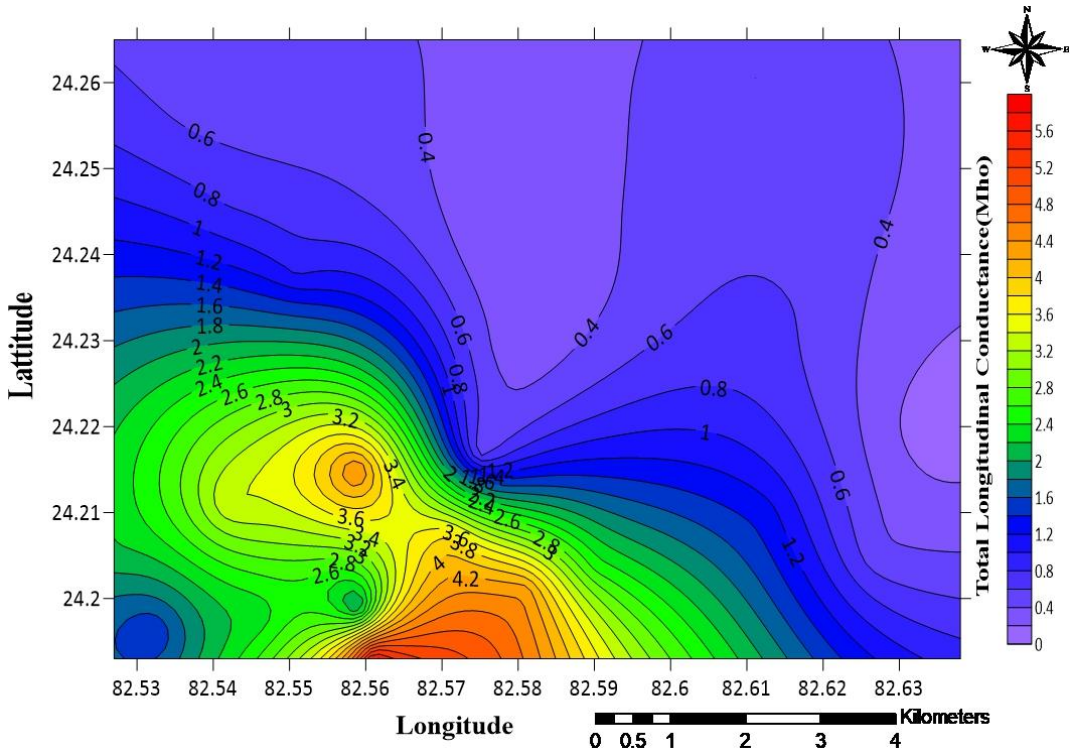

(a)

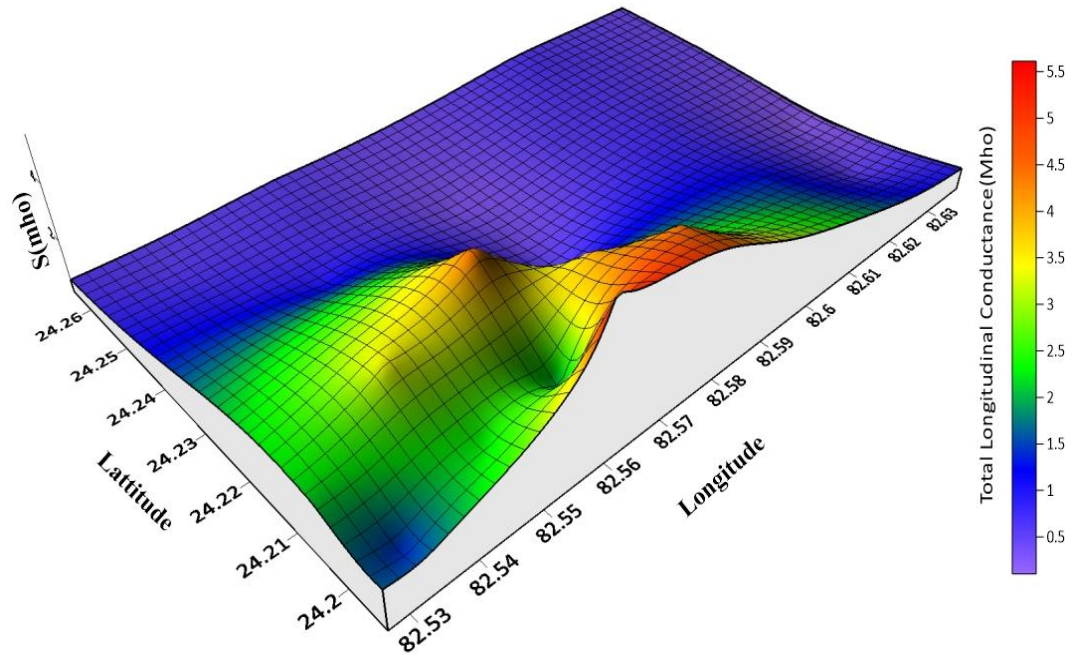

(b)

Figure 6.23 Total longitudinal conductance (S) map (a) 2D Contour map of S,(b) 3D surface map of S.

Overburden Protective capacity

According to Henriet (1976), the ability of an overlying layer to protect against the movement of pollutants by slowing them down and filtering them is directly related to its thickness and inversely related to its hydraulic conductivity. Clayey materials are characterized by low permeability, low resistivity, low hydraulic conductivity, and low longitudinal unit conductance values. Therefore, the protective capacity can be considered proportional to the longitudinal conductance (S). In other words, areas with higher longitudinal conductance in the overburden exhibit a greater protective capacity (Mohammed et al., 2012). The zones can be categorized into various levels of protective capacity, ranging from excellent to poor, based on the values of longitudinal conductance (Oladapo and Akintorinwa, 2007), as given in Table 6.4.

Table 6.4 Longitudinal Conductance/Protective capacity rating (Oladapo and Akintorinwa, 2007)

Longitudinal conductance (mho)	**Protective Capacity Rating**
>10	Excellent
5-10	Very good
0.7-4.9	Good
0.2-0.69	Moderate
0.1-0.19	Weak
<0.1	Poor

By observing Figure 6.23, the contour map and 3D surface map of total longitudinal conductance(S), it is found that a significant portion of the study area has an S value greater than 0.4 mhos, except for some patches on the northern and eastern

sides. So a substantial part of the study area has moderate to very good protective capacity. Hence, most of the study area aquifer is well protected from contaminants.

Total longitudinal Resistivity (ρ_l) Map

Longitudinal resistivity was calculated up to the upper surface of the basement rock using the equation (6.31). The study area (ρ_l) value varies between 5.46 to 708.02 ohm-m. The contour map and 3D surface map of (ρ_l) are shown in Figure 6.24(a) and (b), respectively. The contour map shows that a significant portion of the study area has (ρ_l) less than 250 ohm-m. Only small patches of the area on the eastern side have (ρ_l) greater than 250 ohm-m. These portions can be observed as a peak on 3D surface map.

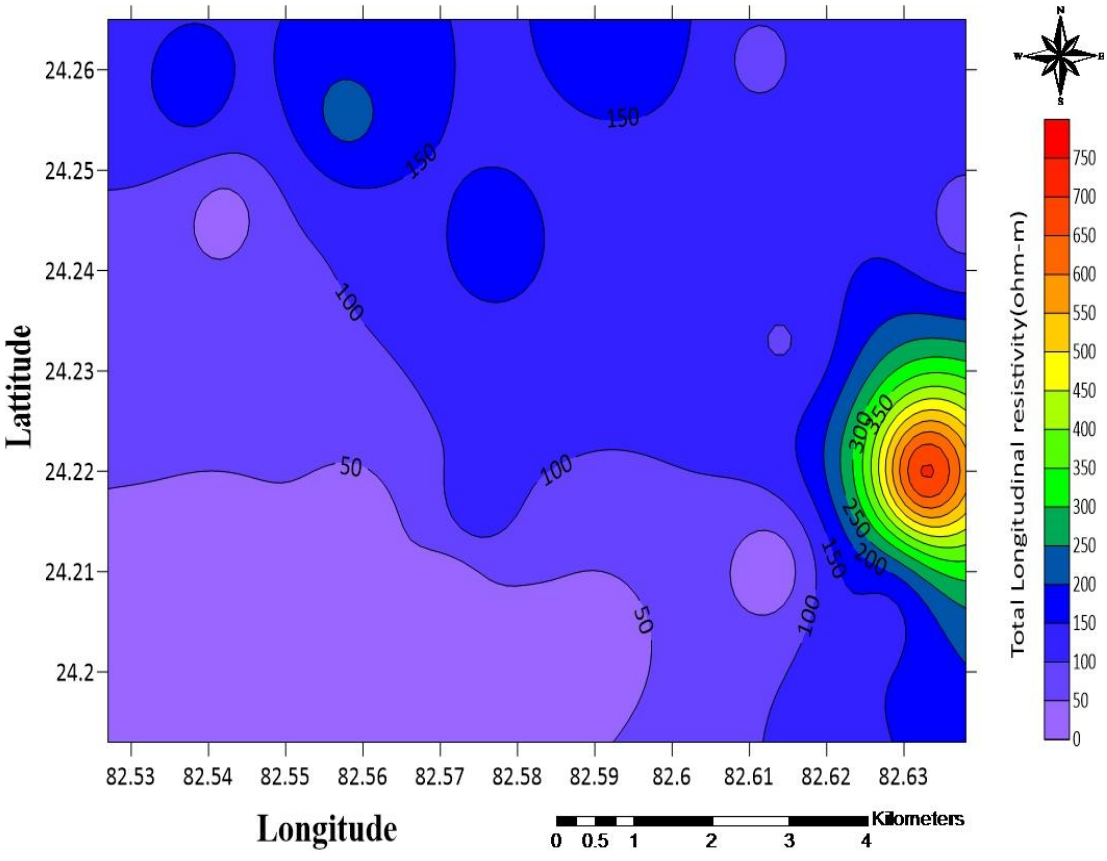

(a)

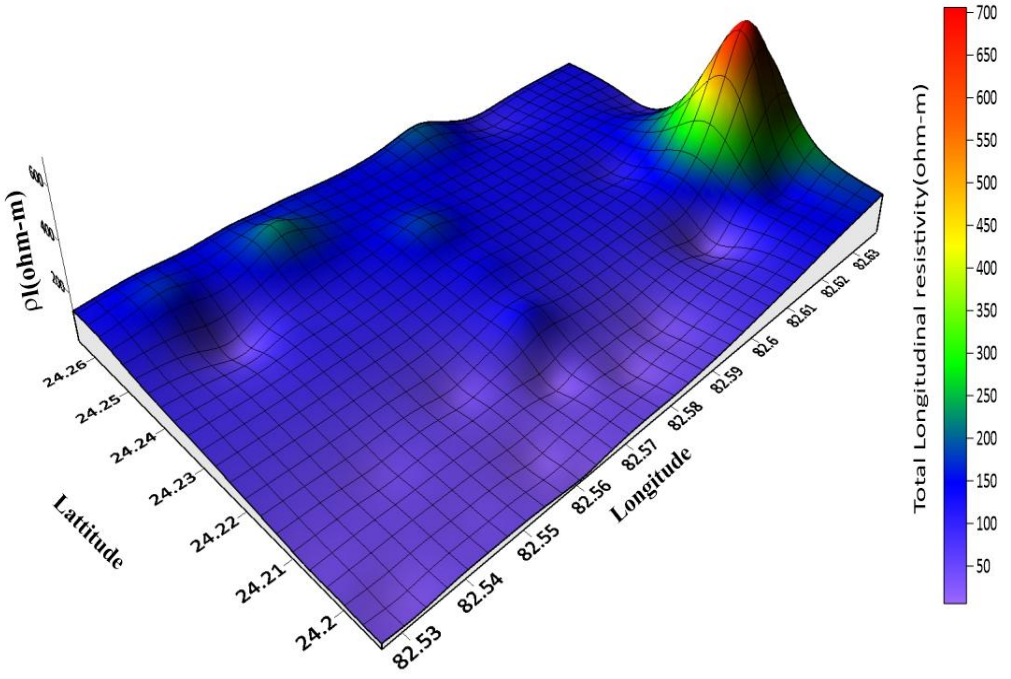

(b)

Figure 6.24. Total longitudinal Resistivity (ρ_l) map (a) 2D Contour map of (ρ_l), (b) 3D Surface map of (ρ_l).

Total Transverse Resistivity (ρ_t) Map

The value of transverse resistivity was estimated up to the top of the basement rock using the equation (6.30), and the value ranges between 9.92 to 3261.53 ohm-m. The total transverse resistivity map of the study area and 3D surface map of (ρ_t) are shown in Figure 6.25(a) and (b). By analyzing the contour map, it can be inferred that about 80% of the area has (ρ_t) less than 1000 ohm-m. Only some portion of the study areas in the north-eastern and eastern sides has (ρ_t) greater than 1000 ohm-m. These regions occur as sharp peaks in 3D surface maps. Salem (1999) stated that (ρ_t) in general is greater than (ρ_l), which was also observed in the present work (Table 6.3). This depicts that the average hydraulic conduction and current flow along the lithological boundary (longitudinal) are greater than those normal (transverse) to the boundary plane. These are geoelectric inhomogeneity as illustrated by Murali and Patangay (1998).

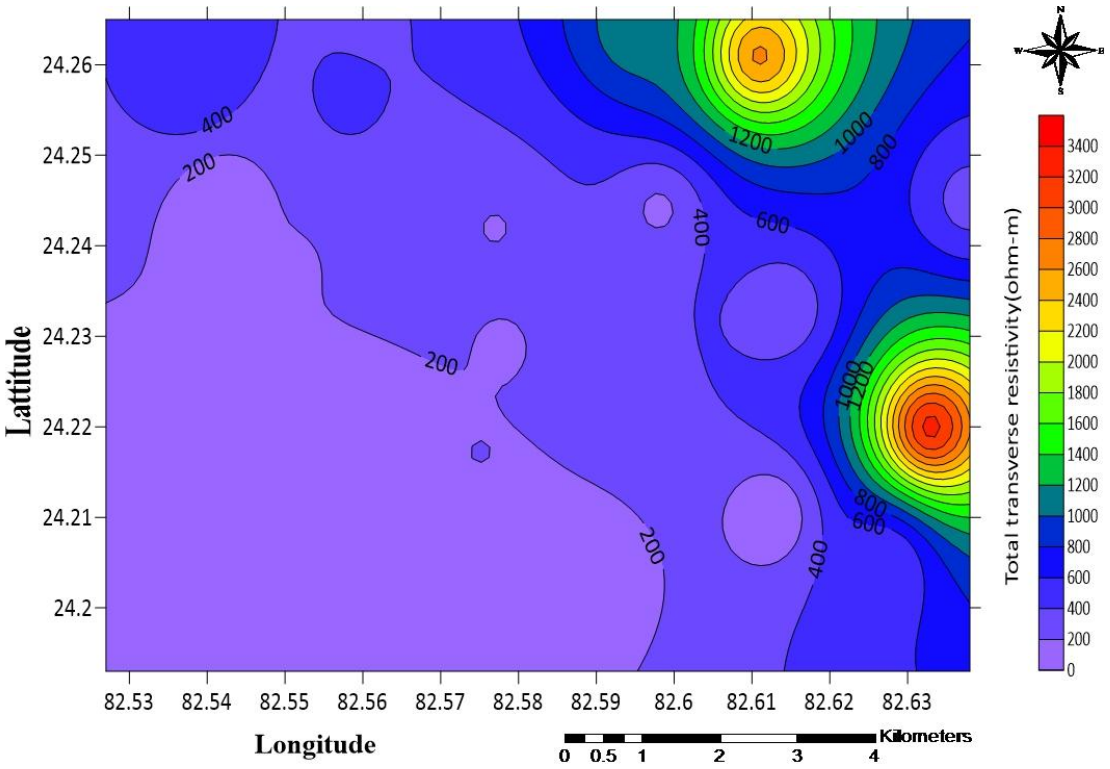

(a)

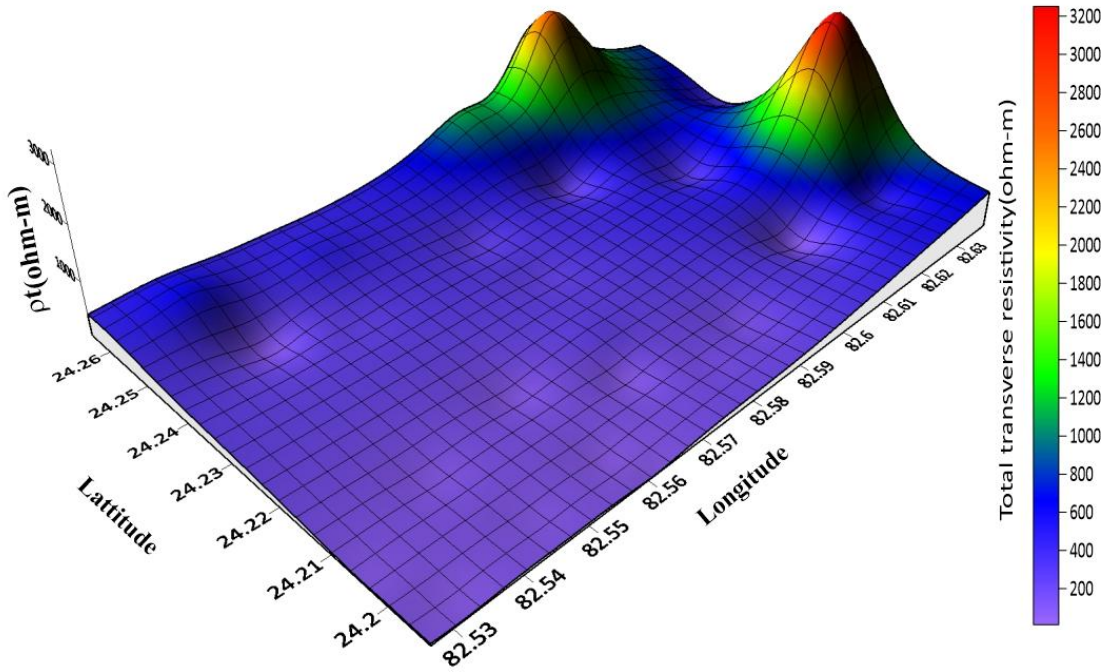

(b)

Figure 6.25 Total Transverse Resistivity (ρ_t) Map (a) 2D Contour map of (ρ_t), (b) 3D Surface map of (ρ_t).

Coefficient of Anisotropy (λ) Map

The concept of coefficient of anisotropy, introduced by the longitudinal and transverse resistivity and serves as a measure of the heterogeneity in a basement terrain. This heterogeneity arises from near-surface effects, varying degrees of weathering, and structural features like fractures, joints, faults, foliations, and beddings (Ayuk et al., 2013). The coefficient of anisotropy is calculated to the top of the basement rock using equation (6.32), and the corresponding map is presented in Figure 6.26.

In the study area, the value of the coefficient of anisotropy varies from 1.02 to 5.34, providing a means to differentiate the groundwater potential zones in the study area. Areas with values between 1.0 to 1.5 are considered as good groundwater potential zones with high porosity and permeability. This is well-collaborated with the work of Rao et al. (2003) which found that areas with anisotropy from 1 to 1.5 are areas with high porosity and permeability, hence considered as good groundwater potential zones. The anisotropy coefficient map is classified into groups based on the observed values. Areas with an anisotropy coefficient of less than one and between 1 to 1.5 are classified as low and good groundwater zone respectively (Ndatuwong and Yadav, 2015). From the contour map and 3D surface map it is observed that 90% of the survey area has a coefficient of anisotropy between 1 to 1.5, so these regions are considered good groundwater potential zones. The remaining part of the map shows a value that is greater than 2 which is associated with low porosity and permeability (Keller and Frischknecht 1966). These are seen as peaks in a 3D surface map.

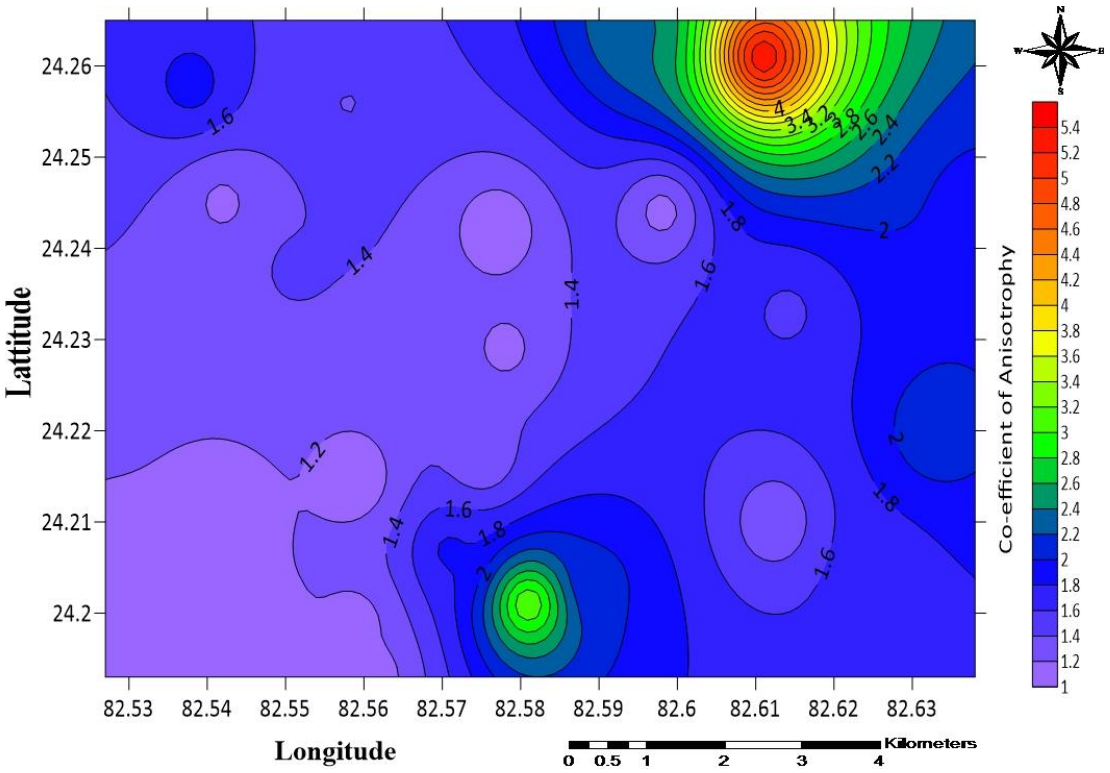

(a)

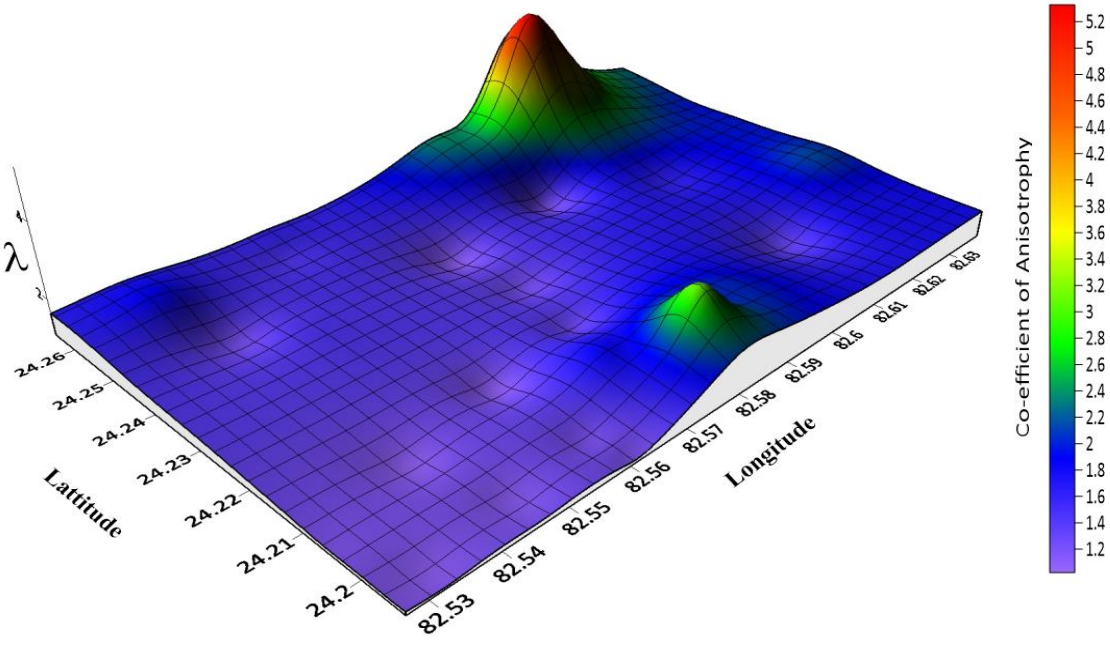

(b)

Figure 6.26 Map of Coefficient of Anisotropy (λ) (a) 2D Contour map of (λ), (b) 3D Surface map of (λ).

6.7.1.4 Identification of Aquifers and Recommendation for the construction of tube wells/dug wells.

The hydrogeological weathered material, forming the overburden, possesses good porosity and contains a large amount of water. However, it exhibits low permeability because of its high clay content (Barker, 2001). On the other hand, the underlying bedrock is fresh but often fractured, resulting in high permeability. However, since fractures do not constitute a significant volume of the rock, the fractured basement has low porosity. Consequently, to obtain a reliable and sustainable water supply from a borehole, the borehole must penetrate a substantial thickness of weathered overburden, which acts as a reservoir. Additionally, the borehole should intersect fractures within the underlying bedrock, as these fractures serve as pathways for rapid water movement (Krishnamurthy et al., 2008).

The weathered/fracture zone is identified in the study area based on the interpretation of fifty-five VES data **(Appendix B)**, and suitable recommendations for constructing tube well and dug well are presented in Table 6.5.

Table 6.5 Identification of Aquifers and Recommendation for tube wells/dug wells

VES NO.	Location	Aquifer	Aquifer thickness	Recommendations
1	Near Kakri colony	Wd S.St to less compact S.St	>20m	Can be considered for tube wells/dug well
2	Near Beena colony	Wd S.St to less compact S.St	>20m	Can be considered for tube wells/dug well
3	Near north of Koharauliya	Wd S.St	>20m	Can be considered for tube wells/dug well
4	Koharauliya-1	Wd S.St to less compact S.St	>20m	Can be considered for tube wells/dug well
5	Koharauliya-2	Wd S.St to less compact S.St	>20m	Can be considered for tube wells/dug well
6	Koharauliya-3	Less to more compact S.St	>20m	Can be considered for tube wells/dug well
7	East of GVP Sagar-1	Wd to semi wd S.St	>20m	Can be considered for tube wells/dug well
8	East of GVP Sagar-2	Wd S.St	>40m	Can be considered for deep tube wells/dug well
9	Near Moher Block	Less compact S.St	<2.5m	Cannot be considered for tube wells/dug wells
10	Near Motwani dam	Highly to less wd S.St	>40m	Can be considered for deep tube wells/dug well
11	Near khadiya colony	Highly to semi wd S.St	>40m	Can be considered for deep tube wells/dug well
12	Near Dudhichu	Wd S.St	>20m	Can be considered for tube wells/dug well
13	Near Bareja Lake	Wd S.St	<5m	Can be considered for dug well only
14	Near Nigahi Internal OB VP	Less compact S.St	<20m	Can be considered for dug well only
15	Near West Turra	Semi Wd S.St	>20m	Can be considered for tube wells/dug well
16	Near Amlohri Colony	Wd to less compact S.St	>20m	Can be considered for tube wells/dug well
17	Near Jayant Colony	Highly wd to semi wd S.St	>40m	Can be considered for deep tube wells/dug well
18	Banauli-1	Highly wd to less wd S.St	>20m	Can be considered for tube wells/dug well
19	Banauli-2	Highly wd to less wd S.St	>20m	Can be considered for tube wells/dug well
20	Banauli-3	Highly wd to less wd S.St	>20m	Can be considered for tube wells/dug well

21	Banauli-4	Highly wd to less wd S.St	>20m	Can be considered for tube wells/dug well
22	SC Nigahi Colony	Highly wd to semi wd S.St	>20m	Can be considered for tubewells/dugwell
23	Nigahi Colony Stadium	Wd to semi S.St	>20m	Can be considered for tube wells/dug well
24	Near Nigahi road	Wd to semi S.St	>20m	Can be considered for tube wells/dug well
25	Amlohri Basti	Wd to semi S.St	>20m	Can be considered for tube wells/dug well
26	Near Ghurital	Highly wd S.St	>20m	Can be considered for tube wells/dug well
27	Near Pachkhora road	Wd S.St	>20m	Can be considered for tube wells/dug well
28	Waidhan	Wd S.St	>20m	Can be considered for tubewells/dugwell
29	Near Mangalam Waidhan	Wd S.St	>20m	Can be considered for tube wells/dug well
30	Singrauli village	Semi wd S.St	<10m	Can be considered for dug well only
31	Khatas	Fractured/Wd Schist	<6.8	Can be considered for dug well only
32	Mahdahiya	Wd S.St	>40m	Can be considered for deep tube wells/dug well
33	Padri	Wd S.St	<20m	Can be considered for dug well only
34	Rampurua	Wd to semi Wd S.St	>40m	Can be considered for deep tube wells/dug well
35	Inurra	Fractured/Wd Schist or shale	>20m	Can be considered for tubewells/dugwell
36	Naudiya	Highly wd S.St	<13m	Can be considered for dug well only
37	Phulzar	Semi wd to less compact S.St	>40m	Can be considered for deep tube wells/dug well
38	Gorbi Basti	Fractured/Wd Schist	<14m	Can be considered for dug well only
39	Khirwa	Fractured/Wd Schist	<5m	Can be considered for dug well only
40	Gorbi block -b colony	Wd S.St	>20m	Can be considered for tube wells/dug well
41	Rajkhand	Semi wd S.St	<10m	Can be considered for dug well only
42	Naudia	Highly to semi wd S.St	<20m	Can be considered for dug well only
43	solang	Wd S.St	>20m	Can be considered for tube

				wells/dug well
44	Kasar	Fractured/Wd Schist	>40m	Can be considered for deep tube wells/dug well
45	Barhati	Wd to semi S.St	<13m	Can be considered for dug well only
46	Lotan	Semi to less compact S.St	>20m	Can be considered for tube wells/dug well
47	Barwani	Semi wd S.St	>20m	Can be considered for tube wells/dug well
48	Piparkhad	Wd/fracture S.St	<20m	Can be considered for tube wells/dug well
49	Karaila	Less compact S.St	>40m	Can be considered for deep tube wells/dug well
50	Bhaudar	Wd S.St	<10m	Can be considered for dug well only
51	Pipra	Wd to compact S.St	>40m	Can be considered for deep tube wells/dug well
52	Gangi	Highly to less wd S.St	<20m	Can be considered for dug well only
53	Tikuritola	Wd S.St to less compact S.St	>40m	Can be considered for deep tube wells/dug well
54	Thurua	Highly to semi wd S.St	>40m	Can be considered for deep tube wells/dug well
55	Ramgarh	Wd to semi wd S.St	>40m	Can be considered for deep tube wells/dug well

Wd=Weathred, S.St=Sandstone

From the above table, it is concluded that most of the VES locations in the study area have semi-weathered to highly weathered Sandstone as aquifers except someplace Villages in the northern region, i.e., Kasar, Ingura, and Kathas. The aquifer thickness at most places varies between 20-40m, which is suitable for constructing tube wells and dug wells.

The comprehensive study presented in this chapter clearly inferred that the Weathered/fractured zones are present in the study area. The lithological information from VES data in the study area shows good agreement with the available borehole lithology. The vertical geoelectrical cross-section gives information about the

lithological changes in subsurface geology along a traverse line. Estimation of Dar-Zarrouk parameters for aquifer characterization in 25 villages around the Gorbi area is used to generate different types of hydro-resistivity contour maps, i.e., total transverse resistance (T), total longitudinal conductance (S), overburden thickness, and coefficient of anisotropy (λ) which are found to be very informative for finding different hydrological information of the area. The total longitudinal conductance map show moderate to very good aquifer protective capacity in the study area and thus indicating the possibility of freshwater aquifers. An overburden thickness map prepared based on the total thickness of soil cover, including clay, sands, and highly weathered to semi-weathered sandstone filled up to the bedrock, indicates the presence of a good aquifer (groundwater bearing zone) wherever thick soil cover is present.

Based on interpreted VES data, fracture/weathered zone are identified at fifty-five sounding stations, and finally, recommendations are given for the construction of tube wells and dug wells. Hence we can say that the VES survey saves time and money in identifying the suitable place to construct tube wells and dug wells. Finally, it can be inferred that the above study is very fruitful in identifying hydrogeological and hydrological knowledge of the study area.